# nature chemistry

**Article** 

https://doi.org/10.1038/s41557-023-01214-0

# Activity-based directed evolution of a membrane editor in mammalian cells

Received: 22 April 2022

Accepted: 24 April 2023

Published online: 22 May 2023

Check for updates

Reika Tei 📵 1,2, Saket R. Bagde 📵 2,3, J. Christopher Fromme 📵 2,3 & Jeremy M. Baskin © 1,2

Cellular membranes contain numerous lipid species, and efforts to understand the biological functions of individual lipids have been stymied by a lack of approaches for controlled modulation of membrane composition in situ. Here we present a strategy for editing phospholipids, the most abundant lipids in biological membranes. Our membrane editor is based on a bacterial phospholipase D (PLD), which exchanges phospholipid head groups through hydrolysis or transphosphatidylation of phosphatidylcholine with water or exogenous alcohols. Exploiting activity-dependent directed enzyme evolution in mammalian cells, we have developed and structurally characterized a family of 'superPLDs' with up to a 100-fold enhancement in intracellular activity. We demonstrate the utility of superPLDs for both optogenetics-enabled editing of phospholipids within specific organelle membranes in live cells and biocatalytic synthesis of natural and unnatural designer phospholipids in vitro. Beyond the superPLDs, activity-based directed enzyme evolution in mammalian cells is a generalizable approach to engineer additional chemoenzymatic biomolecule editors.

Cellular membranes have myriad functions, ranging from being selectively permeable barriers to platforms for initiating signalling pathways<sup>1,2</sup>. Although membranes contain hydrophobic proteins and glycoconjugates<sup>3</sup>, by far their most abundant constituents are lipids. Understanding how each individual lipid constituent contributes to the specific properties and functions of membranes remains a major challenge in membrane biology, one that requires tools for altering the lipid content of endogenous membranes with high molecular and spatiotemporal precision<sup>4</sup>. Akin to how single amino-acid substitutions via site-directed mutagenesis or amber suppression have transformed our ability to perform structure-function relationships within the proteome<sup>5,6</sup>, controllable lipid-modifying enzymes can serve as 'membrane editors' to enable the selective manipulation of individual lipid species within membranes<sup>7,8</sup>.

This strategy has seen the most success with the phosphoinositides, a family of phosphorylated derivatives of phosphatidylinositol, where chemical- or light-induced proximity has been harnessed to create a suite of tools for rapid phosphorylation/dephosphorylation of the inositol head group in situ $^{9-13}$ . Although critically important for many signalling pathways, phosphoinositides are rare lipids, and similar tools for membrane editing beyond this tiny sector of the lipidome are scant<sup>4</sup>. Phosphatidylcholine (PC) is the most abundant lipid within cellular membranes, and we envisioned that it could serve as a substrate for a general membrane editor capable of replacing the choline head group with natural and unnatural head groups to create a wide array of desired phospholipids on demand.

Phospholipase D (PLD) is an ideal starting point for such a general phospholipid membrane editor. PLD catalyses the hydrolysis of PC to form a signalling lipid, phosphatidic acid (PA)14,15, and it can also catalyse transphosphatidylation with exogenous alcohols to swap out head groups to form a variety of natural and unnatural phospholipids<sup>16–19</sup>. Although mammalian cells have endogenous PLD enzymes, they are dispensable for viability and exhibit low levels of basal activity<sup>16</sup>. We have previously identified a microbial PLD that possesses hydrolysis and transphosphatidylation activities in mammalian cells and is amenable to light-mediated control of its localization and activity<sup>20</sup>. However,

Department of Chemistry and Chemical Biology, Cornell University, Ithaca, NY, USA. Weill Institute for Cell and Molecular Biology, Cornell University, Ithaca, NY, USA. 3Department of Molecular Biology and Genetics, Cornell University, Ithaca, NY, USA. A: e-mail: jeremy.baskin@cornell.edu

the activity of this PLD in mammalian cells is modest due to its acidic pH maximum and multiple disulfide bonds<sup>21,22</sup>, limiting its utility to circumstances where very low levels of PA formed by hydrolysis are sufficient to induce a signalling outcome. Thus, we envisioned applying directed evolution to develop super-active PLDs (superPLDs) that would be highly efficient membrane editors for PC hydrolysis to PA and transphosphatidylation to other phospholipids.

Directed enzyme evolution is typically performed as an iteration of two basic steps that mimic natural selection: random or targeted mutagenesis of a gene to generate a library of variants and identification of rare variants that exhibit a desired function through selection or screening<sup>23,24</sup>. Where feasible, selection is preferred to screening, to increase throughput<sup>25</sup>. In vivo selections are typically performed using *Escherichia coli* or *Saccharomyces cerevisiae* as host cells, even when the evolved enzyme is ultimately intended for use in mammalian cells. However, this approach can be problematic for lipid-modifying enzymes, as their substrates are components of membranes, whose compositions and properties differ substantially between bacteria, fungi and higher eukaryotes<sup>26,27</sup>. In these cases, directed evolution in mammalian cells, despite the extra challenges that it brings, is warranted<sup>28</sup>.

Although activity-based labelling is commonly used for directed enzyme evolution, it is typically implemented either in vitro or with cell surface display in bacterial or yeast cells<sup>23,29</sup>. In this Article we overcome substantial technical challenges to develop a directed enzyme evolution strategy for PLD in mammalian cells that harnesses a bioorthogonal, activity-based imaging method for fluorescently tagging cellular membranes proportional to PLD activity. Using this platform, we obtained a series of superPLDs that perform targeted membrane editing up to 100 times more efficiently than wild-type PLD. SuperPLDs exhibit greatly enhanced stability in intracellular environments, which is probably a major contributor to their enhanced performance as membrane editors. Structural and biochemical analysis revealed that superPLDs possess an expanded active site that allows greater access of water and alcohol substrates and are less reliant upon intramolecular disulfides. Because of their substantially improved intracellular stability and activity in cells, superPLDs open up applications both in cell biology for membrane editing of the phospholipidome and in biotechnology for the biocatalytic production of commodity and designer phospholipids. Moreover, our demonstration of activity-based directed enzyme evolution in mammalian cells sets the stage for the engineering of other chemoenzymatic labelling systems in mammalian cells.

#### Results and discussion

#### Activity-based directed evolution of PLD in mammalian cells

We have previously identified PLD from *Streptomyces* sp. PMF for heterologous expression in mammalian cells and developed a light-controlled, optogenetic version of it (optoPLD; Extended Data Fig. 1)<sup>20</sup>. Although optoPLD enabled production of PA or certain phosphatidyl alcohol lipids with organelle-level precision, it exhibited very modest activity, compromising its temporal resolution, and it only accepted a limited set of alcohol substrates. To improve its activity, we first used PLD-expressing yeast cells for directed evolution<sup>20</sup>. However, the fluorescence activated cell sorting (FACS)-based selection was inefficient due to the yeast cell wall, which prevented efficient entry and rinse-out of labelling reagents into live and even fixed cells. Consequently, this platform did not yield PLD mutants with substantially enhanced activity compared to PLD<sup>WT</sup>; the best-performing mutant, G429D, was only 1.3-fold better than PLD<sup>WT</sup>. Therefore, we turned to directed evolution in mammalian cells.

Our activity-based directed evolution strategy in mammalian cells comprises four fundamental steps (Fig. 1). First, a PLD library with random mutations is generated by error-prone polymerase chain reaction (PCR), using either WT or G429D as a template, and then cloned into a lentiviral vector containing the optoPLD system, which

enables blue-light-dependent PLD activation mediated by CRY2–CIBN dimerization<sup>30</sup> to recruit PLD to a desired membrane (Extended Data Fig. 1). Second, lentivirus containing this optoPLD library is generated and delivered into HEK 293T cells such that each cell expresses a different optoPLD mutant. Third, activity-based fluorescent labelling is performed using a bioorthogonal labelling method termed Imaging PLD Activity with Clickable Alcohols via Transphosphatidylation (IMPACT)<sup>31,32</sup> (Fig. 2a). Fourth, cells are sorted by FACS based on the IMPACT fluorescence intensity normalized to optoPLD expression, with IMPACT-high cells collected and propagated.

After one or two cycles of IMPACT and FACS sorting, the enriched PLD library is isolated by DNA extraction and PCR amplification. Subsequent rounds of evolution, with or without additional mutagenesis, are performed while increasing stringency by lowering the concentration of the IMPACT labelling reagent azidopropanol (Extended Data Fig. 2a–s). Overall, we performed three rounds of selection with mutagenesis to increase library diversity and, critically, then five rounds without additional mutagenesis to remove false-positive populations, leading to a dramatic enrichment of highly active PLD mutants (Fig. 2b).

After the final round of selection, we isolated 216 individual clones of the enriched library (in two batches) and found that 194 (90%) exhibited higher activity than PLD^{WT} using IMPACT labelling to assess the activity of these mutant PLDs within an optoPLD system. These mutants exhibited a wide range of activities, with the highest active mutant, clone 2–48, exhibiting -100× higher activity than PLD^{WT} (Fig. 2c,d and Extended Data Fig. 2t–v). Due to this substantial improvement in performance in cells, we denoted these mutants as superPLDs.

# SuperPLD is an efficient hydrolase and transphosphatidylase

Having obtained PLD mutants with a wide-ranging degree of transphosphatidylation activities to generate fluorescent lipids via IMPACT, we next assessed their ability to catalyse PC hydrolysis to form PA and transphosphatidylation to form other useful phospholipids (Fig. 2a). To test superPLD-mediated PA production in cells, we used a PA-binding probe, GFP-PASS<sup>33</sup>, to visualize the subcellular localizations of PA. An optoPLD construct containing the highest active superPLD (2-48; superPLD<sup>high</sup>) exhibited substantial light-independent background activity in cells (Extended Data Fig. 2w-x), resulting in increased cytotoxicity under certain conditions, for example, stable expression following lentiviral transduction. Therefore, we generated optoPLDs bearing moderately active superPLDs (superPLD<sup>low</sup> and superPLD<sup>med</sup>, made from 1-4 and 1-12 with approximately 10× and 30× higher IMPACT  $labelling\,efficiency\,than\,PLD^{WT}in\,mammalian\,cells, respectively)\,capada and the properties of the$ ble of being recruited to either the plasma membrane or lysosomes upon light activation (Fig. 3a). Liquid chromatography mass spectrometry (LC-MS) analysis of transphosphatidylation reactions revealed that superPLD<sup>med</sup> activation consumed ~2-4% of PC in cells, and the total PC levels did not change significantly, probably due to continuous replenishment from biosynthesis (Extended Data Fig. 3a,b). With plasma membrane-targeted optoPLDs, superPLD<sup>low</sup> and superPLD<sup>med</sup>, but not PLDWT, efficiently recruited GFP-PASS to the plasma membrane (Fig. 3b and Extended Data Fig. 3c). Similarly, superPLD<sup>low</sup> and super-PLD<sup>med</sup> greatly outperformed PLD<sup>WT</sup> in lysosome-targeted optoPLD constructs (Fig. 3c and Extended Data Fig. 3d,e).

To evaluate PLD activity in vitro, we purified His-tagged superPLDs expressed in the *E. coli Rosetta 2* strain (Extended Data Fig. 4a). Notably, PLD<sup>WT</sup> was unable to be purified in this manner until switching to *E. coli Rosetta-gami 2*, an engineered strain that facilitates disulfide bond formation in the cytosol<sup>34</sup>, consistent with this PLD being a secreted protein with four disulfide bonds (Extended Data Fig. 4b)<sup>16,35</sup>. Super-PLDs with higher efficiencies in mammalian cells were generally able to be purified in greater yield from a conventional *E. coli* strain (Extended Data Fig. 4c), suggesting that a source of improved superPLD performance is an enhanced stability in intracellular, reductive environments.

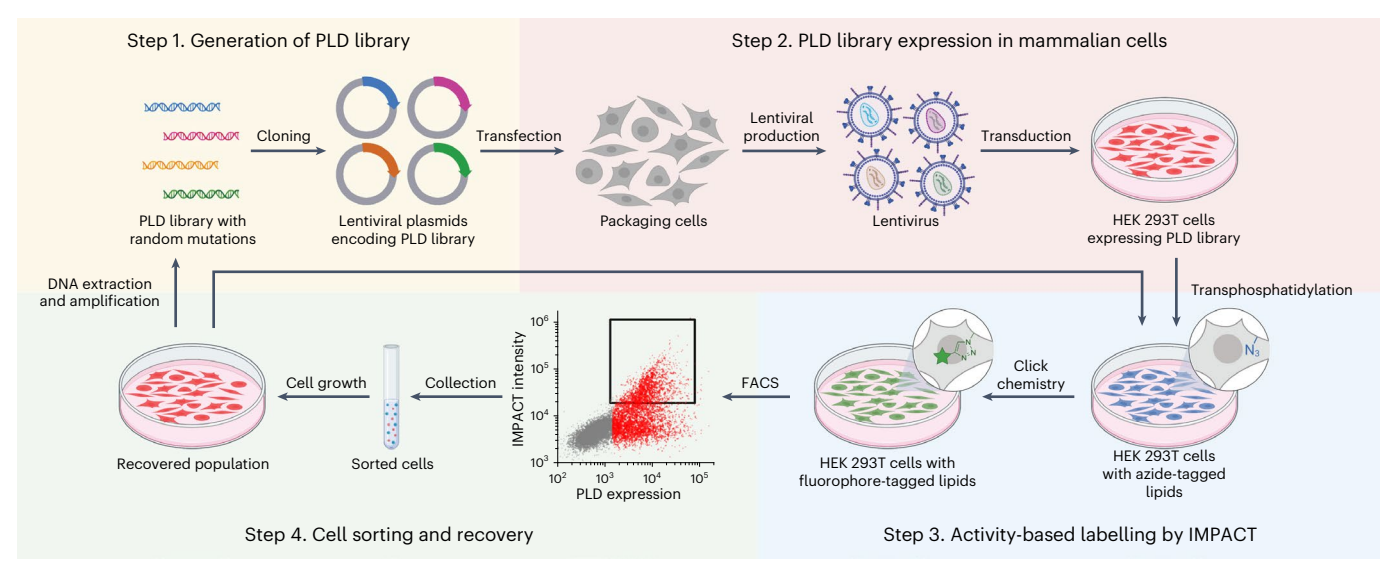


Fig. 1 | Design of an activity-dependent directed enzyme evolution strategy to create a phospholipase D (PLD)-based membrane editor in mammalian cells. Step 1: PLDs with random mutations are generated by error-prone PCR and inserted into a lentiviral optoPLD plasmid. Step 2: packaging cells are transfected with the lentiviral plasmids to produce lentivirus encoding the optoPLD library, which is then transduced into HEK 293T cells. Step 3: cells expressing

the optoPLD library are labelled with IMPACT to fluorescently tag cellular membranes based on the catalytic activity of PLD. Step 4: cells with high IMPACT labelling intensity are isolated by FACS, expanded, and then either the labelling is repeated to better enrich IMPACT-high cells or DNA is extracted and amplified for further rounds of evolution or clonal isolation and sequencing. Schematics were created with BioRender.com.

Supporting this hypothesis, the activity increase of superPLD was much more substantial in cells than in vitro, and superPLD exhibited enhanced chemical stability compared to  $PLD^{WT}$  (Fig. 2d and Extended Data Fig. 4d-h).

Given that, traditionally, transphosphatidylation by PLDs is preferred to hydrolysis <sup>22,36</sup>, we evaluated the ability of superPLD as a catalyst for the in vitro synthesis of a variety of phospholipids from PC and alcohol substrates. By quantifying both PA and phosphatidyl alcohol products by LC–MS, we found that superPLD could be successfully used for the synthesis of various useful natural and unnatural phosphatidyl alcohols derived from both primary and secondary alcohols, with minimal PA by-products formed (Fig. 4). Notably, several unnatural phospholipids with reactive handles such as azide<sup>31</sup> and alkyne<sup>37</sup> could be synthesized with high selectivity and yield. These studies demonstrate the utility of superPLD as a biocatalyst to efficiently produce natural and unnatural phospholipids in in vitro chemoenzymatic reactions.

### SuperPLD modulates PA-dependent signalling pathways

Relative to traditional genetic or pharmacological approaches, membrane editing with optoPLDs offers key advantages to study the direct effects of PA, because optoPLD localization and activity can be engineered orthogonally to and with activities comparable to or perhaps exceeding those of endogenous systems<sup>20</sup>. To establish the general ability of superPLDs to generate physiologically active PA pools, we assessed optogenetic versions of superPLD for the modulation of three different PA-dependent signalling pathways. First, we confirmed that PA made at the plasma membrane by superPLD<sup>med</sup> can attenuate the Hippo growth restriction pathway by triggering translocation of Yes-associated protein (YAP) from the cytosol to the nucleus in serum-starved cells (Extended Data Fig. 5a,b), as we had previously shown for the WT form of optoPLD<sup>20</sup>.

In addition to Hippo signalling, PA can regulate two additional pathways related to nutrient sensing and cell growth: mammalian target of rapamycin (mTOR) signalling<sup>38,39</sup> and AMP-activated protein kinase (AMPK) signalling<sup>40,41</sup>. PA binds to liver kinase B1 (LKB1), which phosphorylates AMPK to activate it<sup>41</sup>; however, such effects counteract the direct stimulatory effect of PA on mTOR signalling due to crosstalk

between AMPK and mTOR signalling (Fig. 5a). To verify these findings and assess the ability of optoPLDs to induce LKB1 translocation to PA-rich membranes, we co-expressed GFP-tagged LKB1 and optoPLDs in HEK 293T cells. Strikingly, PA production on lysosomes by superPLD, but not by PLD<sup>WT</sup>, was sufficient to trigger LKB1 recruitment to lysosomes, consistent with the reported LKB1-PA interaction 41 (Fig. 5b,c).

We then transduced HEK 293T cells with optoPLD using lentivirus and analysed the effects on PA signalling by western blot, in these instances targeting optoPLD to the plasma membrane to mimic the localization of endogenous PLDs when they are stimulated  $^{16,18}$ . Although, as expected, the cells had basal levels of AMPK phosphorylation  $^{42,43}$ , PA production by superPLD led to a significant increase in p-AMPK (Fig. 5d and Extended Data Fig. 5c). The observed 1.3-fold increase in p-AMPK levels with superPLD  $^{\rm med}$  is in agreement with a previous study that reported a twofold increase in p-AMPK levels upon overexpression of human PLD2 in HeLa cells  $^{41}$ . In that study, LKB1 and its cofactor STRAD  $\alpha$  were co-overexpressed to boost the effects of LKB1-mediated AMPK signalling, whereas we isolated LKB1-mediated effects by suppressing CaMKK-mediated AMPK signalling, which might explain the modest discrepancy in the observed fold changes.

Although PA is well documented to positively regulate mTOR signalling, most studies have used either loss-of-function methods (that is, PLD inhibitors or siRNA) or bulk dosing of PA by exogenous addition to cells <sup>39,44–48</sup>. The scarcity of targeted gain-of-function studies using PLD overexpression probably arises from the difficulty in expressing active mammalian PLD enzymes in serum-starved cells, in which most mTOR signalling assays are performed. In a few examples where PLDs were expressed in cells without starvation, p-S6K levels increased twofold (in COS-7 cells) <sup>49</sup> and 1.5-fold (in myotubes) <sup>50</sup>, although no difference was seen in HeLa cells <sup>41</sup>. Using optogenetic superPLDs, we found that, under conditions when AMPK signalling was inhibited with dorsomorphin to reduce crosstalk with mTOR signalling, PM-targeted superPLDs indeed increased phosphorylation of the mTOR effector S6 kinase by more than 1.5-fold (Fig. 5e and Extended Data Fig. 5d).

 $Collectively, these results demonstrate that PA made by opto PLDs can independently activate mTOR and AMPK signalling, and importantly, superPLDs elicited a much stronger response than PLD^{WT} in both$ 

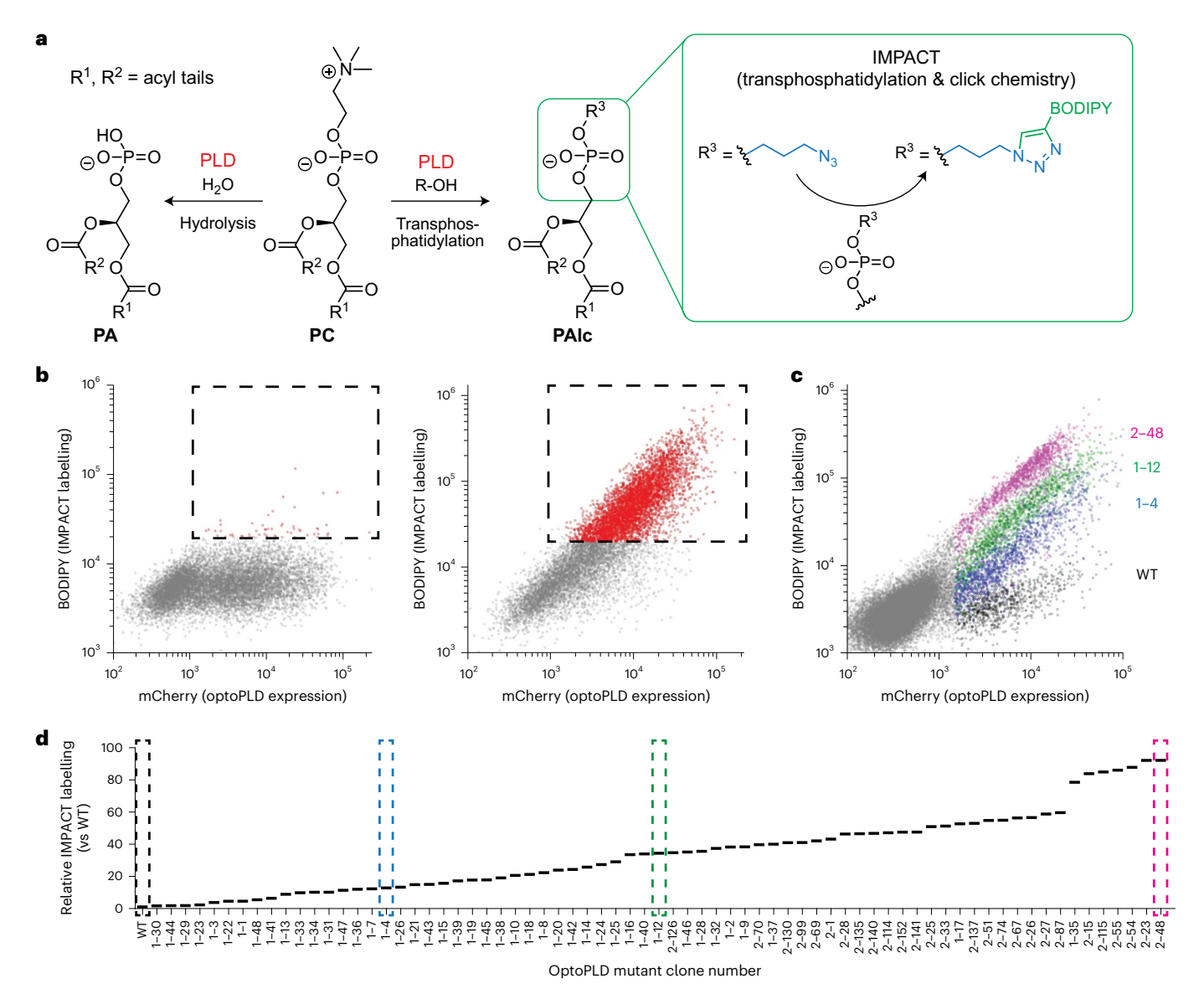


**Fig. 2** | **Directed evolution yields PLD mutants with greatly enhanced activities. a**, Reactions catalysed by PLD, including hydrolysis (left) and transphosphatidylation (right) by using water and alcohols as substrates, respectively. For IMPACT, transphosphatidylation is used to produce azidetagged phospholipids, which are then reacted with a bicyclononyne-BODIPY probe to fluorescently tag the lipids produced by PLD. b, FACS plots showing signal enrichment before (left) and after (right) five rounds of selection without mutagenesis. Red dots marked by dashed boxes indicate cells that were collected. c, Overlay of the FACS plots of cells expressing different optoPLD

mutants. Coloured dots indicate cells expressing PLD<sup>WT</sup> (black), 1-4 (blue), 1-12 (green) and 2-48 (magenta). **d**, Relative PLD activity of representative plasma membrane-targeted optoPLD mutants obtained by directed evolution. IMPACT fluorescence intensity normalized to optoPLD expression was determined by flow cytometry, and the activities are plotted as relative IMPACT labelling of the indicated PLD mutant compared to PLD<sup>WT</sup>. Dashed boxes highlight the four PLD variants (WT, 1-4 (superPLD<sup>low</sup>), 1-12 (superPLD<sup>med</sup>), and 2-48 (superPLD<sup>high</sup>)) characterized in  $\bf c$ .

cases. These studies establish optogenetic superPLDs as general, useful tools for acute manipulation of mammalian PA-dependent signalling pathways, far exceeding what is possible with the original optoPLD.

#### Several mutations cooperate to enhance superPLD activity

We next sought to characterize the mutations that led to increased PLD activity in the superPLDs. Sequencing analysis revealed that each superPLD clone carried five to eleven mutations (Extended Data Fig. 6a). In addition to the G429D mutation present in one of the two templates, the selection produced a few other mutations present in many superPLDs (A258T, G381V and T450A). The generation of mutant PLDs containing some or all of these four mutations only produced modest improvements, in a multiplicative manner, over

 $PLD^{WT}$ , suggesting likely founder effects for these common mutations (Extended Data Fig. 6b).

To dissect the effects of a broader set of mutations, we constructed individual point mutants in two backgrounds, WT and G381V, which was present in all superPLD clones, and assayed their activity (Extended Data Fig. 7a). Individual mutations had variable effects on PLD activity, ranging from a slight decrease to an up to approximately sevenfold increase, with no magic bullet mutation able to recapitulate the activity of the best superPLDs. A minority of mutations did not follow a multiplicative pattern, for example, G406S, which did not increase PLD activity alone but caused a threefold increase in mutant backgrounds (Extended Data Fig. 7a–c). We classified mutations into three groups: (1) mutations that consistently increased

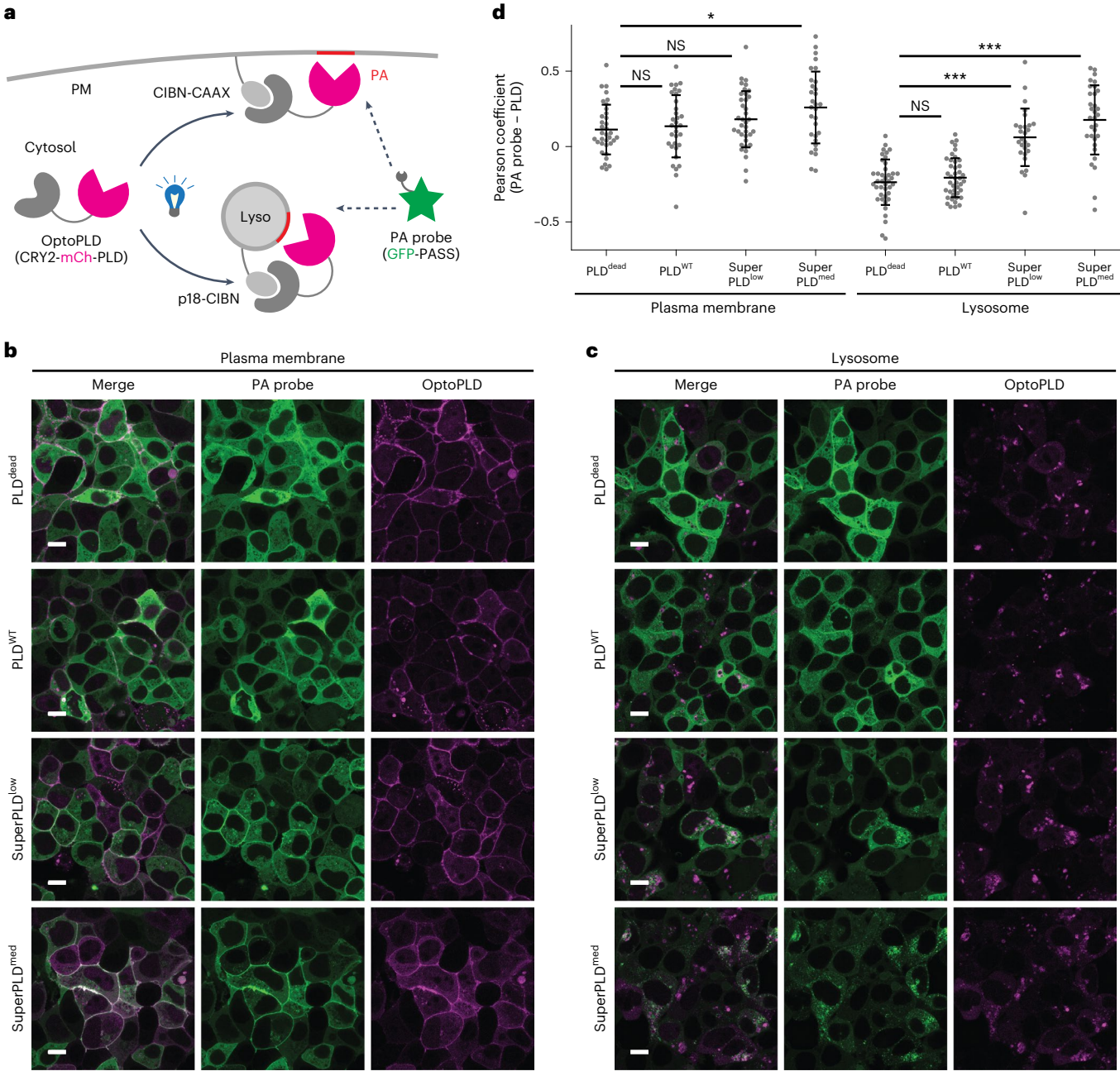


**Fig. 3** | **Evaluation of superPLD activity in cells. a**, Schematic depicting the experimental design of targeting optoPLD to the plasma membrane (PM) or lysosomes (Lyso) and using the PA probe GFP-PASS to visualize PA produced by optoPLD. **b,c**, Confocal images of HEK 293T cells co-expressing the PA probe and optoPLD targeted to the plasma membrane (**b**) or lysosomes (**c**) after 30-min incubation with 488-nm light. **d**, Quantification of colocalization between the PA probe and optoPLD. The plots show the Pearson's correlation coefficient of the PA probe and optoPLD. Black horizontal lines indicate the mean, and vertical error bars indicate the standard deviation (n = 35, 33, 37, 30, 40, 42,

27 and 32, respectively, where n refers to the number of cells examined over three independent experiments). PLD<sup>dead</sup>, a catalytically dead PLD bearing the H167A mutation; PLD<sup>wT</sup>, wild-type PLD; superPLD<sup>low</sup>, superPLD mutant clone 1–4; superPLD<sup>med</sup>, superPLD mutant clone 1–12. Scale bars, 10  $\mu$ m. Statistical significance was determined by one-way analysis of variance (ANOVA) followed by Sidak's multiple comparisons test. \*P < 0.05; \*\*\*P < 0.001; NS, not significant. The P values for the indicated pairwise comparisons are 1.0, 0.50, 0.033, 0.92, < 0.0001 and < 0.0001, respectively.

PLD activity in various backgrounds, (2) mutations that consistently decreased PLD activity or had negligible effects, and (3) mutations that exhibited divergent effects on activity alone versus in mutant backgrounds (Extended Data Fig. 7d). Collectively, this mutational analysis established that the strong effects on superPLD activity are due to the cooperative effect of multiple mutations, most of which are far from the enzyme active site, based on the crystal structure of PLD<sup>WT</sup> (ref. 51).

#### X-ray analysis of superPLD reveals an expanded active site

To investigate how the three-dimensional (3D) structure of superPLD might affect its mechanism, we performed X-ray crystallography on the two most active mutants, 2–23 and 2–48, with structures determined at resolutions of 1.91 and 1.85 Å, respectively (Fig. 6 and Extended Data Fig. 8a–b). Despite sharing only five out of nine mutations, these two superPLDs had structures that were nearly identical to one another but, in certain key ways, different from the reported PLDWT structure 51,52.

Entry	R <sup>3</sup>	PAIc yield (%)	PA yield (%)	Entry	R <sup>3</sup>	PAIc yield (%)	PA yield (%)
1	₹—H	_	84	6	25	65	12
2	₹ NH <sub>2</sub>	98	2	7	35	99	<1
3	°Z√OH OH O	95	2	8	75/	98	<1
4	YZ OH	52	30	9	₹ <b>~</b> N <sub>3</sub>	99	<1
5	HOOH	1 78	15	10	75///	98	<1

**Fig. 4** | **Synthesis of designer phospholipids by in vitro reaction.** The reactions were performed in a biphasic system of ethyl acetate (EtOAc,  $80~\mu$ L) and phosphate-buffered saline (PBS, pH 7.4,  $100~\mu$ L) with 0.8~mg dioleoyl phosphatidylcholine (DOPC),  $0.1~\mu g$  superPLD high (2–48) and  $200~\mu$ mol (for

entries 1–6) or 50  $\mu$ mol (for entries 7–10) alcohol. The PAlc and PA yields indicate the percent conversion of DOPC to dioleoyl phosphatidyl alcohol (DOPAlc) and dioleoyl phosphatidic acid (DOPA), respectively.

Although, overall, the three structures were largely similar, there were major changes in four flexible loops that form the entrance to the active site (Extended Data Fig. 8). In the superPLD structures, two flexible loops near the lipid head group binding site (loops 1 and 4) were farther away from the active site, causing a wider opening than in  $PLD^{WT}$ . However, the two loops closer to the lipid acvl tail binding site (loops 2 and 3) were slightly closer to the active site compared to their positions in PLD<sup>WT</sup>. Critically, the positions of three bulky aromatic residues within loops 1 and 4 (W186, Y190 and Y383) were substantially shifted in the superPLD structures, creating extra space in the catalytic pocket (Fig. 6a-e; note that Y383 is not resolved but its movement is inferred by examining the position of H440, which occupies the position occupied by Y383 in the PLDWT structure). Overall, we consider that the changes to loops 1-4, which delineate the active-site opening at the enzyme-membrane interface, are an important factor that leads to an expanded catalytic pocket where the lipid head group binds, enabling greater access of water and alcohols to the active site and contributing to the increased activity of superPLDs.

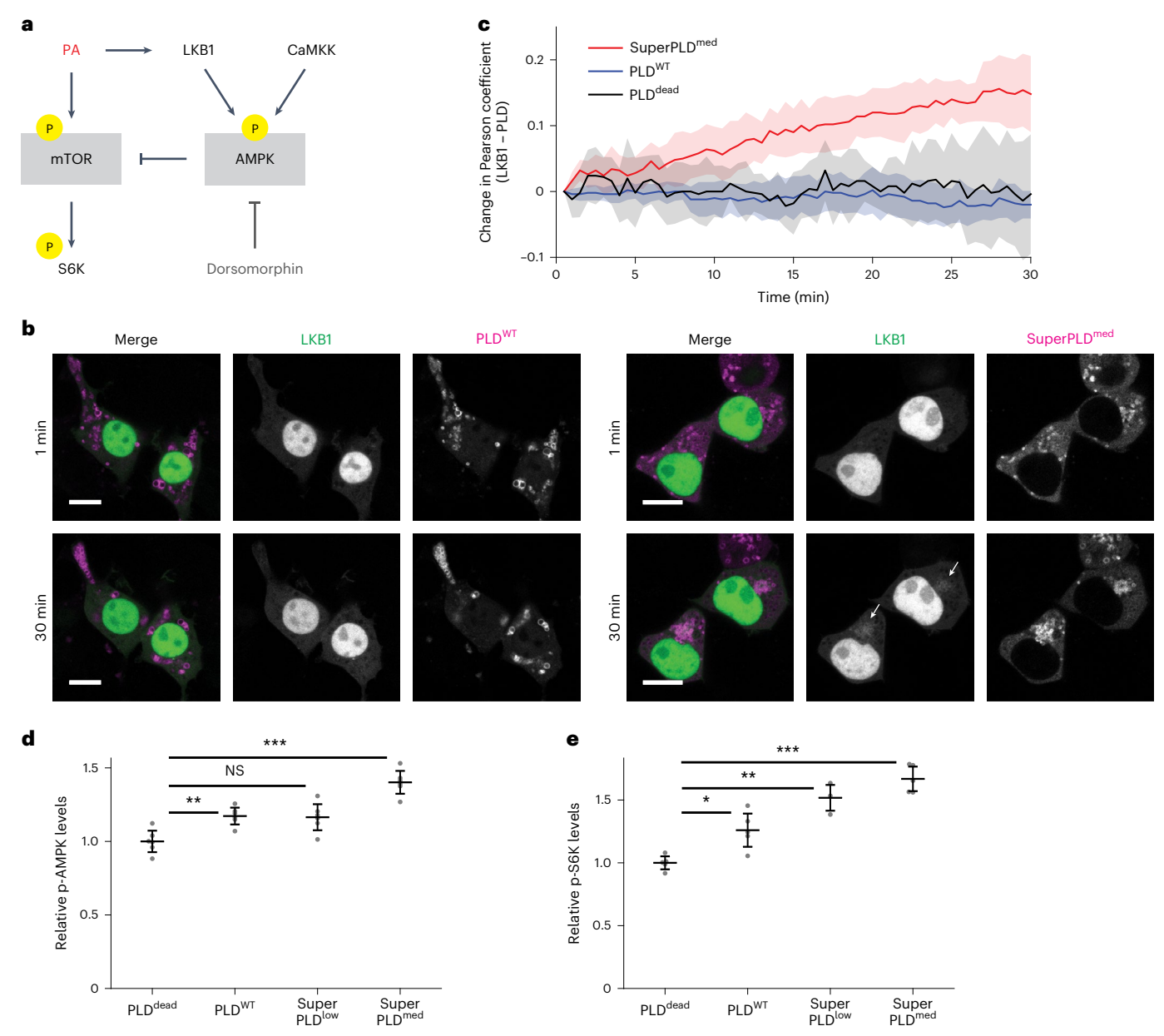
A second difference between superPLD and PLD<sup>WT</sup> inside the catalytic pocket is the orientation of H440, which has flipped away from the active site in the superPLD structures relative to its position in the PLD<sup>WT</sup> structure (Fig. 6c). As H440 directly participates in the reaction mechanism as a general acid/base catalyst (along with the catalytic nucleophile H167)<sup>52,53</sup>, the flipped position of H440 most probably represents the post-catalytic form of superPLD. Consistent with this hypothesis, we found that superPLD co-purified with its product PA, with the electron density of the glycerophosphate head group located between H167 and H440 but at distances too far from either histidine residue for any productive catalysis (Extended Data

Fig. 9a–d). Mutational analysis of superPLD confirmed that residues known to be important for catalysis in PLD were equally important in superPLD, indicating that superPLD most probably shares a similar ligand-binding site as PLD tinits active form (Extended Data Fig. 9e).

Finally, the structural and mutational analysis revealed that superPLD was less reliant on its four intramolecular disulfide bonds than PLDWT. First, the C295-C341 disulfide bond present in PLDWT was absent in superPLD (Extended Data Fig. 10a-d). Second, mutagenesis revealed that superPLD retained its activity much better than PLDWT when the C415-C504 disulfide bond was removed (Fig. 6f). Interestingly, we noticed that the most active superPLDs (2-23 and 2-48) contained two nearby Gly-to-Ser mutations in short unstructured turns or loops adjacent to helices or sheets (G328S and G406S). We postulated that these mutations might favour folding via inter-strand contacts, even in the absence of covalent crosslinking provided by the disulfide, due to reduced entropy from a more restricted conformational space (Extended Data Fig. 10e). Indeed, reversion of those residues to Gly within the superPLD background rendered the enzyme equally sensitive to C415S mutation as PLDWT (Extended Data Fig. 10f,g). Collectively, these analyses point to possible sources of the increased performance of superPLDs in cells and highlight the utility of the mammalian cell-based activity-dependent directed evolution platform for generating superPLDs optimized for use for membrane editing in the reductive environment of cytosol-facing membranes in mammalian cells.

#### **Conclusions**

We have developed an activity-based directed evolution platform in mammalian cells for improving the efficiency and utility of PLD for



**Fig. 5** | **Application of superPLD to manipulate PA signalling. a**, Schematic of the effects of PA on AMPK and mTOR signalling. **b**, Recruitment of GFP-LKB1 triggered by acute PA production on lysosomes by superPLD. GFP-LKB1 and optoPLD (mCherry) fluorescence were measured for 30 min. The experiment was repeated at least three times with similar results, and representative images are shown. Scale bars, 10 μm. **c**, Changes in Pearson correlation coefficient during the recruitment of GFP-LKB1 to optoPLD-positive membranes are plotted for each condition. Solid lines show the mean, and shaded areas indicate the standard deviation (*n* = 5, where *n* refers to the number of cells examined over three independent experiments). **d**, Quantification of phospho-AMPK (p-AMPK) levels in HEK 293T cells with plasma membrane-targeted optoPLDs. Cells were pretreated with a CaMKK inhibitor (STO-609) for 6 h to eliminate CaMKK-mediated AMPK activation, followed by 30-min incubation with intermittent 488-nm light. p-AMPK levels were determined by western blot. Black horizontal

lines indicate the mean, and vertical error bars indicate the standard deviation (n=6 biologically independent samples). Statistical significance was determined by one-way ANOVA followed by Sidak's multiple comparisons test. \*P < 0.05; \*\*P < 0.01; \*\*\*P < 0.001; NS, not significant. The P values for the indicated pairwise comparisons are 0.0012, 0.055 and < 0.0001, respectively. **e**, Quantification of phospho-S6 kinase (p-S6K) levels in HEK 293T cells with plasma membrane-targeted optoPLDs. Cells were pretreated with dorsomorphin for 1 h to eliminate the effects of p-AMPK on mTOR activity, followed by a 30-min incubation with intermittent 488-nm light. p-S6K levels were determined by western blot. Black horizontal lines indicate the mean, and vertical error bars indicate the standard deviation (n=3 for superPLD<sup>low</sup> and n=5 for the others, where n=1 refers to the number of biologically independent samples). Extended Data Fig. 5c,d presents representative western blots. The P values for the indicated pairwise comparisons are 0.038\*, 0.0011\*\* and 0.0001\*\*, respectively.

membrane editing. We have achieved the generation of a series of super-PLDs with a wide range of activities in mammalian cells, with the most active superPLD exhibiting a two-orders-of-magnitude activity increase compared to PLD $^{\rm WT}$ . SuperPLDs efficiently catalysed both hydrolysis and transphosphatidylation of PC, enabling the synthesis of a variety

of natural and unnatural phospholipids with designer head groups. SuperPLDs are poised for use in several types of applications. In cell biology, superPLDs can act as a general membrane editor of the phospholipidome, where products can be dialled in simply by the choice of alcohol substrate<sup>36</sup>. We also envision that recombinant superPLDs will

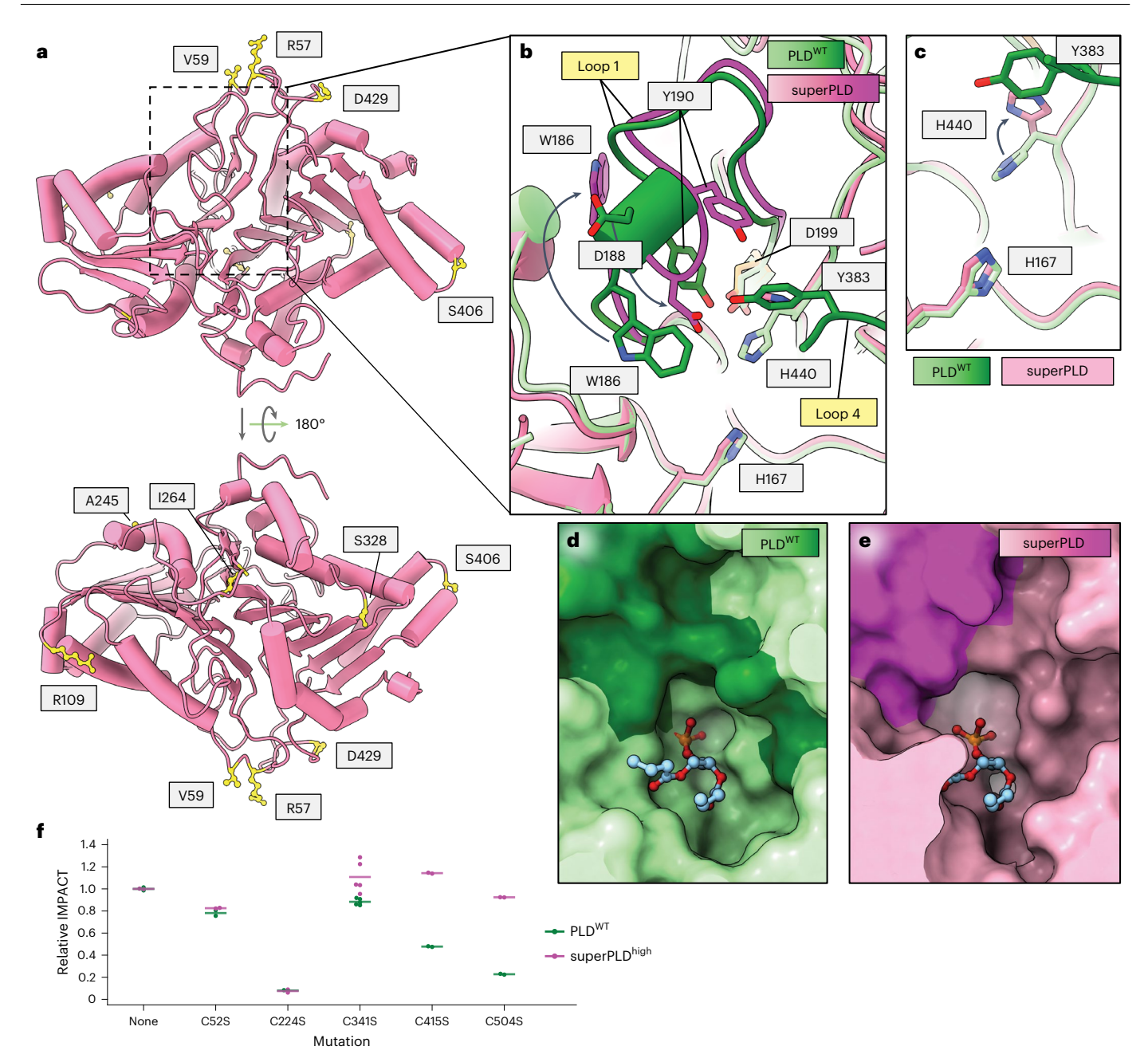


**Fig. 6** | **Structural comparison of superPLD and PLD**<sup>WT</sup>. **a**, Crystal structure of superPLD<sup>high</sup> (2–48). Residues mutated in superPLD are shown in yellow. **b**, Zoomed-in structures around loops 1 and 4. Structures of PLD<sup>WT</sup> and superPLD are shown in green and magenta, respectively, with loops 1 and 4 in each structure shown in a darker colour. **c**, Zoomed-in structures around His 440. **d**,**e**, Surface structures around the catalytic pocket of PLD<sup>WT</sup> (**d**) and superPLD (**e**) highlighting the larger cavity in superPLD. **f**, Comparison of the effect of mutating cysteine residues on PLD<sup>WT</sup> (green) versus superPLD high (2–48; magenta) to prevent

disulfide bond formation. The IMPACT fluorescence intensity normalized to optoPLD expression was determined by flow cytometry. Horizontal lines indicate the average (n=5 for C341S and n=2 for the others, where n refers to the number of independent transfection replicates) of relative mean intensities of IMPACT fluorescence of cells expressing plasma membrane-targeted optogenetic versions of the indicated mutant PLD compared to the parental PLD (for example, PLD<sup>WT</sup> or superPLD<sup>high</sup> (2–48)), as measured by flow cytometry.

be highly desired to replace unoptimized PLDs isolated from natural sources as industrial biocatalysts for the efficient chemoenzymatic synthesis of phospholipids.

The structural and biochemical studies to examine the sources of improved activity of superPLDs compared to PLD<sup>WT</sup> underscore the importance of the activity-based directed evolution strategy in mammalian cells that was used to generate the superPLDs. Each superPLD bears five to eleven mutations, which cooperatively increase enzymatic activity. Instead of targeting residues that directly contact

the substrates, the mutations cause a reorganization of loops that demarcate the active-site opening, leading bulky residues to flip away and create a larger cavity, speaking to the importance of random mutagenesis in our directed evolution strategy. The structural changes in superPLDs also rendered these enzymes more tolerant to disulfide reduction, despite no changes in thermal stability, probably a result of the evolution having been performed in the mammalian cytoplasmic compartment. This latter property also greatly facilitated the purification of superPLDs from *E. coli* in high yield, supporting their

potential development into industrial biocatalysts. We have not, however, observed such variation in PLD<sup>WT</sup> or superPLD expression levels in mammalian cells, perhaps owing to stabilization effects provided by other protein components in the optoPLD scaffold. Furthermore, all quantification of superPLD efficiency in mammalian cells was performed on cell populations expressing the same levels of PLD. Therefore, the improved performance of superPLDs in mammalian cells is not a simple effect caused by increased expression levels.

The highest active superPLDs, when expressed as optoPLDs in mammalian cells, did exhibit higher light-independent background activity, a finding that probably results from our selection platform being focused on engineering higher PLD activity, not necessarily higher fold turn-on by light. Although these superPLDs function well in HEK 293T cells following transient transfection, stable integration has not yet been achieved, probably due to toxicity during prolonged expression, even in the dark. Thus, for studies that require stable expression, further engineering endeavours on the optoPLD scaffold will be required, including exploring alternative optogenetics modules with higher spatiotemporal resolution 54, incorporating inducible expression systems 55, or introducing allosteric regulation mechanisms to directly manipulate enzyme function 56.

Beyond the utility of superPLDs, this study is important for expanding the scope of directed enzyme evolution in mammalian cells to include activity-based fluorescent labelling for enzyme engineering. Metabolic and chemoenzymatic labelling are popular strategies with which to probe or perturb various cellular events, including lipid metabolism<sup>7,57</sup>, glycosylation<sup>58-61</sup>, and other post-translational modifications<sup>62-64</sup>. We envision that extension of our mammalian cell-based directed evolution platform to other enzyme classes will enable the engineering of highly efficient enzymes capable of serving as editors of a wider set of biomolecules in mammalian cells.

#### **Online content**

Any methods, additional references, Nature Portfolio reporting summaries, source data, extended data, supplementary information, acknowledgements, peer review information; details of author contributions and competing interests; and statements of data and code availability are available at https://doi.org/10.1038/s41557-023-01214-0.

#### References

- Harayama, T. & Riezman, H. Understanding the diversity of membrane lipid composition. *Nat. Rev. Mol. Cell Biol.* 19, 281–296 (2018).
- Prinz, W. A., Toulmay, A. & Balla, T. The functional universe of membrane contact sites. Nat. Rev. Mol. Cell Biol. 21, 7–24 (2020).
- 3. Cheng, X. & Smith, J. C. Biological membrane organization and cellular signaling. *Chem. Rev.* **119**, 5849–5880 (2019).
- Tei, R. & Baskin, J. M. Induced proximity tools for precise manipulation of lipid signaling. *Curr. Opin. Chem. Biol.* 65, 93–100 (2021).
- Doudna, J. A. The promise and challenge of therapeutic genome editing. *Nature* 578, 229–236 (2020).
- Porto, E. M., Komor, A. C., Slaymaker, I. M. & Yeo, G. W. Base editing: advances and therapeutic opportunities. *Nat. Rev. Drug Discov.* 19, 839–859 (2020).
- Flores, J., White, B. M., Brea, R. J., Baskin, J. M. & Devaraj, N. K. Lipids: chemical tools for their synthesis, modification and analysis. *Chem. Soc. Rev.* 49, 4602–4614 (2020).
- 8. Tsuchiya, M., Tamura, T. & Hamachi, I. Organelle-selective labeling of choline-containing phospholipids (CPLs) and real-time imaging in living cells. *Curr. Protoc.* **1**, e105 (2021).
- Varnai, P., Thyagarajan, B., Rohacs, T. & Balla, T. Rapidly inducible changes in phosphatidylinositol 4,5-bisphosphate levels influence multiple regulatory functions of the lipid in intact living cells. J. Cell Biol. 175, 377–382 (2006).

- Suh, B.-C., Inoue, T., Meyer, T. & Hille, B. Rapid chemically induced changes of PtdIns(4,5)P<sub>2</sub> gate KCNQ ion channels. Science 314, 1454–1457 (2006).
- Zoncu, R. et al. Loss of endocytic clathrin-coated pits upon acute depletion of phosphatidylinositol 4,5-bisphosphate. *Proc. Natl Acad. Sci. USA* 104, 3793–3798 (2007).
- 12. Hammond, G. R. V. et al. PI4P and  $PI(4,5)P_2$  are essential but independent lipid determinants of membrane identity. Science **337**, 727–730 (2012).
- Idevall-Hagren, O., Dickson, E. J., Hille, B., Toomre, D. K. & Camilli,
   P. D. Optogenetic control of phosphoinositide metabolism. *Proc. Natl Acad. Sci. USA* 109, E2316–E2323 (2012).
- Tanguy, E., Wang, Q., Moine, H. & Vitale, N. Phosphatidic acid: from pleiotropic functions to neuronal pathology. Front. Cell. Neurosci. 13, 2 (2019).
- Athenstaedt, K. & Daum, G. Phosphatidic acid, a key intermediate in lipid metabolism. Eur. J. Biochem. 266, 1–16 (1999).
- Selvy, P. E., Lavieri, R. R., Lindsley, C. W. & Brown, H. A. Phospholipase D: enzymology, functionality and chemical modulation. *Chem. Rev.* 111, 6064–6119 (2011).
- Bumpus, T. W., Liang, F. J. & Baskin, J. M. Ex uno plura: differential labeling of phospholipid biosynthetic pathways with a single bioorthogonal alcohol. *Biochemistry* 57, 226–230 (2018).
- Liang, D. et al. A real-time, click chemistry imaging approach reveals stimulus-specific subcellular locations of phospholipase D activity. Proc. Natl Acad. Sci. USA 116, 15453–15462 (2019).
- Tei, R. & Baskin, J. M. Click chemistry and optogenetic approaches to visualize and manipulate phosphatidic acid signaling. *J. Biol. Chem.* 298, 101810 (2022).
- Tei, R. & Baskin, J. M. Spatiotemporal control of phosphatidic acid signaling with optogenetic, engineered phospholipase Ds. J. Cell Biol. 219, e201907013 (2020).
- Carrea, G. et al. Purification and properties of two phospholipases D from Streptomyces sp. Biochim. Biophys. Acta 1255, 273–279 (1995).
- Yang, H. & Roberts, M. F. Phosphohydrolase and transphosphatidylation reactions of two Streptomyces phospholipase D enzymes: covalent versus noncovalent catalysis. Protein Sci. Publ. Protein Soc. 12, 2087–2098 (2003).
- 23. Wang, Y. et al. Directed evolution: methodologies and applications. *Chem. Rev.* **121**, 12384–12444 (2021).
- Gargiulo, S. & Soumillion, P. Directed evolution for enzyme development in biocatalysis. *Curr. Opin. Chem. Biol.* 61, 107–113 (2021).
- Sheludko, Y. V. & Fessner, W.-D. Winning the numbers game in enzyme evolution—fast screening methods for improved biotechnology proteins. *Curr. Opin. Struct. Biol.* 63, 123–133 (2020).
- van Meer, G. & de Kroon, A. I. P. M. Lipid map of the mammalian cell. *J. Cell Sci.* **124**, 5–8 (2011).
- Kesidis, A. et al. Expression of eukaryotic membrane proteins in eukaryotic and prokaryotic hosts. Methods 180, 3-18 (2020).
- Hendel, S. J. & Shoulders, M. D. Directed evolution in mammalian cells. Nat. Methods 18, 346–357 (2021).
- 29. Könning, D. & Kolmar, H. Beyond antibody engineering: directed evolution of alternative binding scaffolds and enzymes using yeast surface display. *Microb. Cell Fact.* **17**, 32 (2018).
- Kennedy, M. J. et al. Rapid blue-light-mediated induction of protein interactions in living cells. Nat. Methods 7, 973–975 (2010).
- Bumpus, T. W. & Baskin, J. M. Clickable substrate mimics enable imaging of phospholipase D activity. ACS Cent. Sci. 3, 1070–1077 (2017).
- Bumpus, T. W., Liang, D. & Baskin, J. M. IMPACT: imaging phospholipase D activity with clickable alcohols via transphosphatidylation. *Methods Enzymol* 641, 75–94 (2020).

- Zhang, F. et al. Temporal production of the signaling lipid phosphatidic acid by phospholipase D2 determines the output of extracellular signal-regulated kinase signaling in cancer cells. Mol. Cell. Biol. 34, 84–95 (2014).
- 34. Rosano, G. L. & Ceccarelli, E. A. Recombinant protein expression in *Escherichia coli*: advances and challenges. *Front. Microbiol.* **5**, 172 (2014).
- Zambonelli, C. et al. Cloning and expression in Escherichia coli
  of the gene encoding Streptomyces PMF PLD, a phospholipase
  D with high transphosphatidylation activity. Enzyme Microb.
  Technol. 33, 676–688 (2003).
- Allegretti, C., Denuccio, F., Rossato, L. & D'Arrigo, P. Polar head modified phospholipids by phospholipase D-catalyzed transformations of natural phosphatidylcholine for targeted applications: an overview. *Catalysts* 10, 997 (2020).
- Bumpus, T. W. & Baskin, J. M. A chemoenzymatic strategy for imaging cellular phosphatidic acid synthesis. *Angew. Chem. Int.* Ed. 55, 13155–13158 (2016).
- Fang, Y., Vilella-Bach, M., Bachmann, R., Flanigan, A. & Chen, J. Phosphatidic acid-mediated mitogenic activation of mTOR signaling. Science 294, 1942–1945 (2001).
- Frias, M. A. et al. Phosphatidic acid drives mTORC1 lysosomal translocation in the absence of amino acids. *J. Biol. Chem.* 295, 263–274 (2020).
- Mukhopadhyay, S. et al. Reciprocal regulation of AMP-activated protein kinase and phospholipase D. J. Biol. Chem. 290, 6986–6993 (2015).
- 41. Dogliotti, G. et al. Membrane-binding and activation of LKB1 by phosphatidic acid is essential for development and tumour suppression. *Nat. Commun.* **8**, 15747 (2017).
- 42. Vincent, E. E. et al. Differential effects of AMPK agonists on cell growth and metabolism. *Oncogene* **34**, 3627–3639 (2015).
- Vara-Ciruelos, D. et al. Genotoxic damage activates the AMPK-α1 isoform in the nucleus via Ca<sup>2+</sup>/CaMKK2 signaling to enhance tumor cell survival. *Mol. Cancer Res.* 16, 345–357 (2018).
- 44. Fang, Y. et al. PLD1 regulates mTOR signaling and mediates Cdc42 activation of S6K1. *Curr. Biol.* **13**, 2037–2044 (2003).
- Sun, Y. et al. Phospholipase D1 is an effector of Rheb in the mTOR pathway. Proc. Natl Acad. Sci. USA 105, 8286–8291 (2008).
- Yoon, M.-S. et al. Rapid mitogenic regulation of the mTORC1 inhibitor, DEPTOR, by phosphatidic acid. *Mol. Cell* 58, 549–556 (2015).
- 47. Bernfeld, E. et al. Phospholipase D-dependent mTOR complex 1 (mTORC1) activation by glutamine. *J. Biol. Chem.* **293**, 16390–16401 (2018).
- 48. Tei, R., Morstein, J., Shemet, A., Trauner, D. & Baskin, J. M. Optical control of phosphatidic acid signaling. *ACS Cent. Sci.* **7**, 1205–1215 (2021).
- Lehman, N. et al. Phospholipase D2-derived phosphatidic acid binds to and activates ribosomal p70 S6 kinase independently of mTOR. FASEB J. 21, 1075–1087 (2007).
- Jaafar, R. et al. Phospholipase D regulates the size of skeletal muscle cells through the activation of mTOR signaling. Cell Commun. Signal. 11, 55 (2013).
- Leiros, I., Secundo, F., Zambonelli, C., Servi, S. & Hough, E. The first crystal structure of a phospholipase D. Structure 8, 655–667 (2000).

- Leiros, I., McSweeney, S. & Hough, E. The reaction mechanism of phospholipase D from *Streptomyces* sp. strain PMF. Snapshots along the reaction pathway reveal a pentacoordinate reaction intermediate and an unexpected final product. *J. Mol. Biol.* 339, 805–820 (2004).
- Samantha, A., Damnjanović, J., Iwasaki, Y., Nakano, H. & Vrielink, A. Structures of an engineered phospholipase D with specificity for secondary alcohol transphosphatidylation: insights into plasticity of substrate binding and activation. *Biochem. J.* 478, 1749–1767 (2021).
- 54. Benedetti, L. et al. Light-activated protein interaction with high spatial subcellular confinement. *Proc. Natl Acad. Sci. USA* **115**, E2238–E2245 (2018).
- Das, A. T., Tenenbaum, L. & Berkhout, B. Tet-on systems for doxycycline-inducible gene expression. *Curr. Gene Ther.* 16, 156–167 (2016).
- 56. Fauser, J., Leschinsky, N., Szynal, B. N. & Karginov, A. V. Engineered allosteric regulation of protein function. *J. Mol. Biol.* **434**, 167620 (2022).
- Ancajas, C. F., Ricks, T. J. & Best, M. D. Metabolic labeling of glycerophospholipids via clickable analogs derivatized at the lipid headgroup. Chem. Phys. Lipids 232, 104971 (2020).
- Chao, L. & Jongkees, S. High-throughput approaches in carbohydrate-active enzymology: glycosidase and glycosyl transferase inhibitors, evolution and discovery. *Angew. Chem.* 131, 12880–12890 (2019).
- Griffin, M. E. & Hsieh-Wilson, L. C. Glycan engineering for cell and developmental biology. *Cell Chem. Biol.* 23, 108–121 (2016).
- 60. Zeng, Y., Tang, F., Shi, W., Dong, Q. & Huang, W. Recent advances in synthetic glycoengineering for biological applications. *Curr. Opin. Biotechnol.* **74**, 247–255 (2022).
- 61. Hong, S. et al. Glycoengineering of NK cells with glycan ligands of CD22 and selectins for B-cell lymphoma therapy. *Angew. Chem. Int. Ed.* **60**, 3603–3610 (2021).
- 62. Rabuka, D. Chemoenzymatic methods for site-specific protein modification. *Curr. Opin. Chem. Biol.* **14**, 790–796 (2010).
- 63. Garst, E. H., Das, T. & Hang, H. C. Chemical approaches for investigating site-specific protein S-fatty acylation. *Curr. Opin. Chem. Biol.* **65**, 109–117 (2021).
- 64. Suazo, K. F., Park, K.-Y. & Distefano, M. D. A not-so-ancient grease history: click chemistry and protein lipid modifications. *Chem. Rev.* **121**, 7178–7248 (2021).

**Publisher's note** Springer Nature remains neutral with regard to jurisdictional claims in published maps and institutional affiliations.

Springer Nature or its licensor (e.g. a society or other partner) holds exclusive rights to this article under a publishing agreement with the author(s) or other rightsholder(s); author self-archiving of the accepted manuscript version of this article is solely governed by the terms of such publishing agreement and applicable law.

© The Author(s), under exclusive licence to Springer Nature Limited 2023

### Methods

#### Cell culture, transfection and lentiviral transduction

HEK 293T cells were obtained from ATCC (CRL-3216) and HEK 293TN cells were obtained from the Bretscher laboratory (Cornell). Cells were grown in Dulbecco's modified Eagle medium (DMEM; Corning) supplemented with 10% fetal bovine serum (FBS; Corning), 1% penicillin/streptomycin (Corning) and 1 mM sodium pyruvate (Thermo Fisher) at 37 °C in a 5% CO<sub>2</sub> atmosphere. For poly-L-lysine pre-treatment, cell plates were treated with 0.1 mg ml<sup>-1</sup> poly-L-lysine (Sigma Aldrich, P2636) in phosphate-buffered saline (PBS) for 1–12 h at 37 °C, followed by triple rinses with autoclaved deionized water.

For transfection, HEK 293T cells were transfected using Lipofectamine 2000 (Invitrogen, 11668019) following the manufacturer's protocol. Briefly, the cells were incubated in regular DMEM medium containing plasmids pre-mixed with Lipofectamine 2000 (0.3  $\mu g$  of optoPLD plasmid and 0.75  $\mu l$  of Lipofectamine 2000 per well for a 24-well plate), and the cells were incubated for 20–24 h before being labelled and analysed.

For lentivirus production, HEK 293TN cells seeded on a six-well plate were incubated in Transfectagro (Corning) supplemented with 10% FBS containing plasmids pre-mixed with Lipofectamine 2000 (0.5 μg envelope plasmid, 1 μg packaging plasmid, 1.5 μg optoPLD plasmid and 6 µl of Lipofectamine 2000 per well for a six-well plate). At 8 h following transfection, the transfection medium was replaced with regular DMEM medium, and media were collected 24 h and 48 h after transfection to obtain virus-containing medium. For lentiviral transduction, HEK 293T cells seeded on a six-well plate (pretreated with poly-L-lysine) were incubated in 1.5 ml of virus-containing medium supplemented with 0.5 ml of fresh medium and 0.8 µg ml<sup>-1</sup> polybrene (Millipore Sigma). The six-well plate was covered with aluminium foil to keep the cells in the dark. After 24 h, virus-containing medium was replaced with fresh DMEM medium, and the cells were incubated in the dark for another 24 h before being labelled and sorted (details are provided in the IMPACT labelling and cell sorting section).

#### Generation of optoPLD libraries and mutants

Libraries of optoPLD mutants (Supplementary Table 1) were generated by error-prone PCR as described previously<sup>65</sup>. Briefly, 100 ng of the template DNA was amplified with 0.5 µM forward and reverse primers (Supplementary Table 2; primers 10 and 11), 200 µM dNTPs mix. 2 µM 8-oxo-dGTP (TriLink BioTechnologies, N-2034), 2 µM dPTP (TriLink BioTechnologies, N-2037) and 2.5 U of Tag polymerase in Thermopol reaction buffer (New England Biolabs, B9004S). The PCR products were then gel-purified and re-amplified for another 25 cycles under normal PCR conditions using the same primers. The second PCR products were digested using BamHI/EcoRI and cloned into optoPLD lentiviral vector (pCDH-CRY2-mCh-PLD-P2A-CIBN-CAAX; Supplementary Table 1, entry 4) digested using the same restriction enzymes. The ligated product was transformed into DH5α E. coli, and the grown colonies were scraped and subjected to plasmid extraction. The resulting optoPLD plasmids were used to transfect HEK 293TN cells for lentivirus production (details are provided in the Mammalian cell culture, transfection and lentiviral transduction

To introduce site-specific mutations to PLD, N-terminal and C-terminal fragments of PLD were amplified using primer 10 (Supplementary Table 2) and a reverse mutagenizing primer containing a desired mutation (Supplementary Table 3) for the N-terminal fragment, and primer 11 (Supplementary Table 2) and a forward mutagenizing primer (Supplementary Table 3) for the C-terminal fragment. The two fragments were then stitched together using overlap-extension PCR to obtain the mutagenized PLD, which was subsequently cloned into an optoPLD transient expression vector (pCDNA3-CRY2-mCh-PLD-P 2A-CIBN-CAAX; Supplementary Table 1, entry 6) using BamHI and EcoRI cut sites.

#### Set-up for optogenetics experiments

A homemade light box was built by attaching four strips of dimmable, 12-V blue-LED tape light (1000Bulbs.com; 2835–60-IP65-B1203) on the inside of a Styrofoam box. For optogenetics experiments, the light box was placed inside the  $CO_2$  incubator using an a.c. Outlet Power Bank (Omars; 24,000 mAh, 80 W) as a power supply. An outlet timer (BN-LINK) was used to switch the light on and off automatically to enable 3-s intervals of blue light in every 1 min.

#### IMPACT labelling and cell sorting

PLD1/2 double-knockout HEK 293T cells<sup>18</sup> expressing optoPLD libraries were treated with 1-5 mM azidopropanol for 30 min at 37 °C in the presence of intermittent blue-light illumination (3-s pulses every 1 min). After three rinses with PBS, cells were treated with 1 uM bicyclononyne-BODIPY fluorophore (BCN-BODIPY<sup>66</sup>) for 10 min at 37 °C. The cells were again rinsed three times with PBS and incubated in DMEM medium for 10 min at 37 °C to remove excess fluorophore. The cells were then trypsinized, resuspended in PBS, and sorted using a Sony MA900 cell sorter or a FACSAria Fusion cell sorter. Cells expressing optoPLD<sup>dead</sup>, a catalytically dead mutant (H167A), were similarly labelled and sorted as a negative control, and the population in cells expressing optoPLD libraries that showed higher signal than the negative control was collected. The collected cells were expanded, at which point cells were reseeded for another round of selection or subjected to genomic extraction. Flow cytometry plots and histograms showing the sorting strategy and collected cell populations for each round of selection are provided in Extended Data Fig. 2.

#### Genomic extraction and amplification of PLD fragments

Genomic DNA was extracted from HEK 293T cells using a NucleoSpin Blood kit (Takara Bio, 740951) following the manufacturer's protocol. Briefly, cells were rinsed once with PBS and lysed, and then the lysate was applied to the DNA-binding column. After rinsing and drying the column, 60  $\mu$ l of water was applied to elute DNA. The eluate was used as a template for PCR reactions to amplify PLD fragments. For the PCR reactions, 0.5–10  $\mu$ l of template was amplified for 25 cycles under normal PCR conditions with primers 8 and 9 (Supplementary Table 2; for use with Taq polymerase) or primers 10 and 11 (Supplementary Table 2; for use with Phusion polymerase). The PCR products were digested and cloned into the optoPLD vector as described in the Generation of optoPLD libraries section.

# Directed evolution of optoPLDs

For the first round of evolution, two optoPLD libraries were generated using PLD<sup>WT</sup> or PLD<sup>G429D</sup> (the G429D mutation exhibits modestly higher (-1.3-fold) activity than PLD<sup>WT</sup>)<sup>20</sup> as the starting template. The optoPLD libraries were introduced into HEK 293T cells using lentiviral transduction, and cells expressing optoPLD libraries were labelled and sorted as described in the IMPACT labelling and cell sorting section. The sorted cells were expanded before another cycle of IMPACT labelling and cell sorting. After the second cycle of selection, cells were subjected to genomic extraction. The PLD fragments were amplified from the extracted DNA using Taq polymerase to introduce more mutations and then cloned into optoPLD vector.

For the second and third rounds of evolution, the optoPLD libraries were generated using the product of the previous round of evolution as the template. For these rounds, Taq polymerase, which has lower fidelity and is thus expected to introduce approximately one mutation per PLD, was used for amplification. Further mutations were added by error-prone PCR, and the libraries with and without error-prone PCR were combined. The generated optoPLD libraries were expressed in cells, and the cells were labelled and sorted as described above. The sorted cells were subjected to two more cycles of selection, followed by genomic extraction and PLD amplification.

For the fourth and subsequent rounds of evolution, genomic DNA extracted from cells was amplified using Phusion polymerase to minimize the introduction of further mutations. The rest of the evolution was performed similarly.

After evolution, PLD mutants were cloned into an optoPLD transient expression vector (Supplementary Table 1, entry 6) using BamHI and EcoRI cut sites. Each plasmid isolated from a single *E. coli* colony was analysed by Sanger sequencing using primers 28 and 29 (Supplementary Table 2) to determine the mutations in each clone of PLD mutants.

#### Quantitative comparison of PLD activity using IMPACT

HEK 293T cells were transiently transfected with CRY2-mCh-PLD-P2A-CIBN-CAAX, where the PLD sequence contained the indicated set of mutations, and cells were kept in the dark for 18–24 h. For IMPACT labelling, cells were treated with 0.1–1 mM azidopropanol for 30 min at 37 °C in the presence of intermittent blue-light illumination (3-s pulses every 1 min). After three rinses with PBS, the cells were treated with 1  $\mu$ M BCN-BODIPY for 10 min at 37 °C, again rinsed three times with PBS, and incubated in DMEM medium for 10 min at 37 °C. Cells were then trypsinized and subjected to flow cytometry analysis using an Attune NxT flow cytometer to measure mCherry and BODIPY fluorescence, which correspond to optoPLD expression level and IMPACT labelling intensity, respectively. Cells expressing similar amounts of optoPLD were gated, and the average IMPACT signal in the gated population was used to compare the PLD activity of different mutants (Extended Data Fig. 2t).

#### Imaging of PA localization by confocal microscopy

Due to the large size of the DNA encoding CRY2-mCherry-PLD-P2A-CIBN-CAAX, which affected lentivirus production efficiency, CRY2-mCherry-PLD and CIBN-CAAX were packaged into separate lentivirus constructs. pCDH-CRY2-mCherry-superPLD was prepared by cloning superPLD into an optoPLD lentiviral expression vector (Supplementary Table 1, entry 8) using BamHI and EcoRI cut sites. Lentivirus containing GFP-PASS, CRY2-mCherry-PLD, and CIBN-CAAX (for plasma membrane-targeted optoPLD) or p18-CIBN (lysosome-targeted optoPLD) were prepared as described in the Mammalian cell culture, transfection and lentiviral transduction section. Spinfection was used for efficient co-transduction of HEK 293T cells with the three lentivirus preparations. Briefly, cells were seeded on 35-mm glass-bottom imaging dishes (Matsunami Glass) and, after the addition of lentivirus-containing medium to the cells, the cells were centrifuged at 931g for 2 h at 37 °C. After spinfection, the lentivirus-containing medium was replaced with regular growth medium, and the cells were kept in the dark for 48 h before imaging.

For colocalization analysis with LysoView 633, HEK 293T cells transduced with GFP-PASS, CRY2-mCherry-PLD, and p18-CIBN were prepared as described above, and 1X LysoView 633 was added before the imaging. For evaluation of LKB1 localization, HEK 293T cells seeded on imaging dishes were transfected with GFP-LKB1 and p18-CIBN-P2A-CRY2-mCherry-PLD using Lipofectamine 2000, and the cells were kept in the dark for 20 h before imaging.

Images were acquired every 1 min for 1 h at 37 °C using Zeiss Zen Blue 2.3 on a Zeiss LSM 800 confocal laser-scanning microscope equipped with Plan Apochromat objectives (×40, 1.4 NA) and two GaAsP PMT detectors. Solid-state lasers (488, 561 and 640 nm) were used to excite the GFP, mCherry and LysoView 633, respectively, and the 488-nm laser irradiation also served as a stimulus for activating optoPLD recruitment to the plasma membrane or lysosomes. The colocalization between GFP-PASS/LKB1 and CRY2-mCherry-PLD was calculated for each transfected cell using the Coloc 2 plugin on ImageJ.

#### PLD expression from E. coli and purification

The PLD construct was cloned into the pCAV4.1 vector<sup>67</sup> (Supplementary Table 1, entry 13), which is a modified T7 expression

vector containing an N-terminal 6xHis-NusA tag followed by a peptide sequence that is cleavable by the HRV 3C protease. Constructs were transformed into Rosetta 2 (DE3) or Rosetta-gami 2 (DE3) E. coli, grown at 37 °C in 2 × 11 Terrific broth medium supplemented with chloramphenicol (25 μg ml<sup>-1</sup>) and ampicillin (100 μg ml<sup>-1</sup>) to an optical density at 600 nm of 0.8, and then induced with isopropyl-β-D-1-thiogalactopyranoside (0.1 mM) for 20 h at 18 °C. Cells were collected by centrifugation, resuspended in 50 ml of bacterial lysis buffer (50 mM sodium phosphate, 500 mM NaCl, 10% glycerol, pH 7.5) supplemented with 5 mM β-mercaptoethanol (for *Rosetta*) and 0.5 mM phenylmethylsulfonyl fluoride, and homogenized using a sonic dismembrator (Fisherbrand Model 505). The cell lysate was centrifuged at 30,000g for 30 min, and the supernatant was incubated with 2 ml of TALON Metal Affinity Resin (Takara Bio) for 1 h at 4 °C with rotation. The resin was then loaded onto a disposable column (Bio-Rad) and rinsed five times with 25 ml of bacterial lysis buffer. After resuspending the washed resin in 5 ml of bacterial lysis buffer, His-tagged HRV 3C protease was added and the mixture was incubated overnight at 4 °C with rotation to elute PLD from the resin. The supernatant containing cleaved PLD was concentrated using an Amicon 0.5-ml 10-kDa molecular-weight cutoff centrifugal filter. For crystallization and thermal stability analysis, further purification of PLD using size-exclusion chromatography was performed using an ÄKTA pure system equipped with a Superdex 200 Increase 10/300 GL column in 20 mM Tris-HCl (pH 8.0) and 150 mM NaCl.

#### In vitro kinetics assays of PLD activity

PLD activity was determined using an Amplex Red Phospholipase D assay kit following the manufacturer's protocol. Briefly, 100  $\mu$ M Amplex Red, 2 U ml $^{-1}$  horseradish peroxidase, 0.2 U ml $^{-1}$  choline oxidase, and 0.02–0.4 mg ml $^{-1}$  1,2-dioleoyl-sn-glycero-3-phosphatidylcholine (DOPC; prepared 40 mg ml $^{-1}$  in ethanol) were added to PBS (pH 7.4) to prepare a master mix solution. The solution was added to 10 ng ml $^{-1}$  PLD to start the reaction, and fluorescence signal was measured during incubation at 37 °C using a BioTek Synergy H1 microplate reader. The luminescence signal at the reaction endpoint, when all the DOPC was consumed, was used to convert the luminescence signal (a.u.) to [product] ( $\mu$ M) for calculating  $V_{\rm max}$ . The  $K_{\rm m}$  and  $k_{\rm max}$  of the reaction were calculated based on the Michaelis–Menten equation.

#### Phospholipid synthesis and LC-MS analysis

In 1.5-ml Safe-Lock Eppendorf tubes, 50 uM to 2 M of alcohol and 0.1 ug of PLD were added to 100 µl PBS (pH 7.4). For ethanolamine, the pH was adjusted to pH 7.4 by the addition of HCl. After the addition of 0.8 mg of DOPC in 80 µl ethyl acetate, the tubes were placed in a plastic box and shaken vigorously in a 37 °C shaker for 1-24 h at 350 r.p.m. The reaction was quenched by adding 250 μl of methanol, 125 μl of acetic acid (20 mM in water), and 500 µl of chloroform. The solution was mixed thoroughly by shaking vigorously for 5 min, and the tubes were centrifuged at high speed for 1 min, then 10-µl aliquots of the bottom organic layer were collected and transferred into new tubes. The solutions were diluted, filtered, and subjected to high-resolution LC-MS analysis to quantify the concentrations of DOPC, dioleoyl phosphatidic acid (DOPA) and dioleoyl phosphatidyl alcohol (DOPAlc) in the sample. The obtained concentration was used to calculate the total amount of each compound in the reaction mixture, which was used to determine the percent yield for DOPA and DOPAlc.

LC-MS analysis was performed on an Agilent 6230 electrospray ionization–time-of-flight MS coupled to an Agilent 1260 HPLC equipped with a Luna 3- $\mu$ m Silica LC column (Phenomenex; 50  $\times$  2 mm) using a binary gradient elution system in which solvent A was chloroform/methanol/ammonium hydroxide (85:15:0.5) and solvent B was chloroform/methanol/water/ammonium hydroxide (60:34:5:0.5). Separation was achieved using a linear gradient from 100% A to 100% B over 10 min. Phospholipid species were detected using an Agilent

Jet Stream source operating in positive or negative mode, acquiring in an extended dynamic range from m/z 100 to 1,700 at one spectrum per second (gas temperature, 325 °C; drying gas, 12 l min<sup>-1</sup>; nebulizer, 35 psig; fragmentor, 300 V (for positive mode) and 250 V (for negative mode); sheath gas flow, 12 l min<sup>-1</sup>;  $V_{\rm cap}$ , 3,000 V; nozzle voltage, 500 V).

#### Thermal stability analysis

The thermal stabilities of PLD<sup>WT</sup> and superPLDs were determined as previously reported<sup>68</sup>. Briefly, PLD<sup>WT</sup> and superPLDs were diluted to 0.1 mg ml<sup>-1</sup> final concentration in Tris-HCl buffer (10 mM, pH 8.0, 150 mM NaCl) containing SYPRO Orange (1:1,000 dilution of 5,000× concentrate). The fluorescence signal was measured while the temperature was slowly raised using a Roche LightCycler 480 device. The melting temperature ( $T_{\rm m}$ ) was determined by the temperature at which the fluorescence signal reached 50% of its maximum.

#### Chemical stability analysis

The chemical stabilities of PLD<sup>WT</sup> and superPLD<sup>high</sup> (2–48) were determined by measuring the residual activity of PLD treated with urea. PLD (1  $\mu g$  ml $^{-1}$ ) was incubated in solutions of 0–4 M urea in PBS for 12 h at 37 °C, after which the PLD activity was measured as described in the In vitro kinetics assays of PLD activity section. The relative rate of the reaction compared to 0 M urea (untreated) PLD was used to estimate the chemical stability.

#### Evaluation of YAP localization by immunofluorescence

HEK 293T cells seeded on cover glasses coated with poly-L-lysine were transfected with CRY2-mCherry-PLD-P2A-CIBN-CAAX, and the cells were kept in the dark for 16 h before being placed in a serum-starvation medium (DMEM supplemented with 1% penicillin/streptomycin without FBS). After 6 h of starvation, the cells were stimulated for 1 h with intermittent blue-light illumination (5-s pulses every 1 min), followed by cell fixation and immunostaining as described previously20. Briefly, the cells were fixed in 4% paraformaldehyde for 10 min at room temperature, followed by extraction in a solution of 0.5% Triton X-100 in PBS for 5 min. The cells were then blocked in a solution of 1% BSA and 0.1% Tween-20 in PBS (blocking buffer) for 30 min. Immunostaining was then performed by treating the cells with a 1:100 dilution of anti-YAP antibody (Santa Cruz Biotechnology, sc-101199) in blocking buffer for 1 h, rinsing three times with 0.1% Tween-20 in PBS solution (PBS-T), treatment with a 1:1.000 dilution of anti-mouse-Alexa Fluor 488 antibody conjugate (Invitrogen, A-21202) in blocking buffer for 1 h, and rinsing three times with PBS-T. The cells were mounted on microscope slides using ProLong Diamond Antifade Mountant with 4',6-diamidino-2-phenylindole (DAPI; Thermo Fisher) and incubated overnight at room temperature in the dark. Image acquisition by laser-scanning confocal microscopy was performed as described above by using solid-state lasers (405, 488 and 561 nm) to excite the DAPI, Alexa Fluor 488 and mCherry, respectively.

#### Quantification of p-AMPK and p-S6K by western blotting

HEK 293T cells were transduced with CRY2-mCherry-PLD and CIBN-CAAX using lentivirus and spinfection as described in the 'Evaluation of phosphatidic acid localization by confocal microscopy' section. The cells were incubated with either 10  $\mu$ M STO-609 (CaMKK inhibitor; for AMPK signalling assay) for 6 h or 10  $\mu$ M dorsomorphin (AMPK inhibitor; for mTOR signalling assay) for 1 h at 37 °C, followed by 30-min stimulation with intermittent blue-light illumination (5-s pulses every 1 min). The cells were then lysed with RIPA lysis buffer supplemented with protease and phosphatase inhibitors (50 mM Tris-HCl, pH 7.4, 150 mM NaCl, 1% Triton X, 0.5% sodium deoxycholate, 0.1% SDS, 1 mM EDTA, 1× cOmplete Protease Inhibitor, 17.5 mM  $\beta$ -glycerophosphate, 20 mM sodium fluoride, 1 mM activated sodium orthovanadate, 5 mM sodium pyrophosphate). After sonication and centrifugation, the lysate supernatants were mixed with 6× Laemmli sample buffer to

prepare the sample for western blotting. The membrane was blotted with 1:1,000 dilutions of antibodies for phospho-AMPKα (Thr172; Cell Signaling Technology, #2535), phospho-p70 S6 kinase (Thr389; Cell Signaling Technology, #9205), p70 S6 kinase (Santa Cruz Biotechnology, sc-8418), mCherry (Novus Biologicals, NBP1-96752), or actin (MP Biomedicals, 08691001), with detection by chemiluminescence using the Clarity Western ECL substrate (Bio-Rad) and acquisition on a Bio-Rad ChemiDoc MP system.

#### Quantification of substrate conversion by superPLD in cells

HEK 293T cells seeded on 12-well plates were transduced with CRY2-mCherry-PLD and CIBN-CAAX using lentivirus and spinfection as described above. The cells were incubated with 0.5–2% ethanol, which should be sufficient to inhibit most PLD hydrolysis activity $^{22}$ , for 30 min with intermittent blue-light illumination. The cells were then rinsed with PBS three times and subjected to lipid extraction. For lipid extraction, the cells were scraped in 250  $\mu l$  of methanol, 125  $\mu l$  of acetic acid (20 mM in water) and 100  $\mu l$  of PBS. The cell suspension was transferred into a 1.5-ml centrifuge tube, and the lipids were extracted and subjected to LC–MS analysis as described in the 'Phospholipid synthesis and LC–MS analysis' section.

#### Crystallization of superPLD

Crystals for superPLD<sup>high</sup> (2–48 mutant) were obtained by mixing 1  $\mu$ l of purified protein at 2.5 mg ml<sup>-1</sup> with 1  $\mu$ l of well solution containing 21% PEG, 0.15 M Li<sub>2</sub>SO<sub>4</sub> and citrate-NaOH (pH 4.4) and equilibrated against 200  $\mu$ l of well solution at 18 °C. Crystals grew within 5–7 days. Single crystals were collected and soaked in the well solution supplemented with 10% ethylene glycerol for 10 s before plunge-freezing in liquid N<sub>2</sub>. Crystals for the 2–23 superPLD mutant (whose activity in cells is comparable to superPLD<sup>high</sup> (2–48)) were obtained by mixing 1  $\mu$ l of purified protein at 2.5 mg ml<sup>-1</sup> with 1  $\mu$ l of well solution containing 19% PEG, 0.15 M Li<sub>2</sub>SO<sub>4</sub> and citrate-NaOH (pH 4.15) and equilibrated against 200  $\mu$ l of well solution at 18 °C. Crystals grew within 5–7 days. Single crystals were collected and soaked in the well solution supplemented with 10% ethylene glycol for 10 s before plunge-freezing in liquid N<sub>2</sub>.

#### X-ray diffraction data collection, processing and analysis

Diffraction experiments were conducted at beamline 24-ID-E of the Advanced Photon Source (APS) and beamline ID7B2 of the Cornell High Energy Synchrotron Source (CHESS). Diffraction datasets were collected at 100 K and processed using XDS<sup>69</sup>. Crystals of the two super-PLD mutants (superPLD  $^{\rm high}$  (2–48) and 2–23) diffracted to 1.85 Å and 1.9 Å, respectively. The crystal structure of PLDWT (PDB 1VOY) was used to obtain phasing information using molecular replacement using Phaser<sup>70</sup> in PHENIX<sup>71</sup>. The models were subjected to iterative rounds of manual re-building using COOT<sup>72</sup> followed by refinement in PHENIX<sup>71</sup>. We observed electron density in the active site that probably corresponds to a bound reaction intermediate. Based on previously reported structures of PLD in complex with reaction intermediates (PDB 7JRU and 7JRV), we modelled a phosphate moiety in part of this density. We note that the density was not clear enough to model the glycerol backbone and the acyl chains, so we omitted these groups from the model. Final refinement and validation statistics for the models are reported in Supplementary Table 4.

#### **Reporting summary**

Further information on research design is available in the Nature Portfolio Reporting Summary linked to this Article.

#### **Data availability**

Structural models and structure factors of superPLD (2-48) and superPLD (2-23) have been deposited in the RCSB PDB under accession nos. 8CTQ and 8CTP, respectively. The superPLD plasmids used for this

study have been deposited in Addgene (https://www.addgene.org/browse/article/28229113/). Other data supporting the findings of this study are available within the Article and the Supplementary Information. Source data are provided with this paper.

# **Code availability**

Python code used for sequencing data processing, systematic mutational analysis and flow cytometry data processing are available within the Supplementary Information.

#### References

- Angelini, A. et al. Protein engineering and selection using yeast surface display. In Yeast Surface Display: Methods, Protocols and Applications (ed. Liu, B.) 3–36 (Springer, 2015); https://doi. org/10.1007/978-1-4939-2748-7 1
- Alamudi, S. H. et al. Development of background-free tame fluorescent probes for intracellular live cell imaging. *Nat. Commun.* 7, 11964 (2016).
- 67. Bosire, E. M. et al. Diffusible signal factors act through AraC-type transcriptional regulators as chemical cues to repress virulence of enteric pathogens. *Infect. Immun.* **88**, e00226-20 (2020).
- Joiner, A. M. N. & Fromme, J. C. Structural basis for the initiation of COPII vesicle biogenesis. Structure 29, 859–872 (2021).
- 69. Kabsch, W. XDS. Acta Crystallogr. D Biol. Crystallogr. **66**, 125–132 (2010).
- Bunkóczi, G. et al. Phaser.MRage: automated molecular replacement. Acta Crystallogr. D Biol. Crystallogr. 69, 2276–2286 (2013).
- 71. Liebschner, D. et al. Macromolecular structure determination using X-rays, neutrons and electrons: recent developments in Phenix. Acta Crystallogr. D Struct. Biol. **75**, 861–877 (2019).
- Emsley, P., Lohkamp, B., Scott, W. G. & Cowtan, K. Features and development of Coot. Acta Crystallogr. D Biol. Crystallogr. 66, 486–501 (2010).

# **Acknowledgements**

J.M.B. acknowledges support from a Beckman Young Investigator award, a Sloan Research Fellowship and the NSF (CAREER CHE-1749919). R.T. was supported by Honjo International, Funai Overseas and Cornell fellowships. J.C.F. and S.R.B were supported by NIH/NIGMS grant no. R35GM136358. Beamline 24-ID-E of APS is funded by the National Institute of General Medical Sciences from the National Institutes of Health (P30 GM124165). The Eiger 16M

detector on the 24-ID-E beamline is funded by an NIH-ORIP HEI grant (S10OD021527). This research used resources of the Advanced Photon Source, a US Department of Energy (DOE) Office of Science User Facility operated for the DOE Office of Science by Argonne National Laboratory under contract no. DE-AC02-06CH11357. Beamline ID7B2 of CHESS is supported by the NSF under award no. DMR-1829070, and by award no. 1-P30-GM124166-01A1 from the National Institute of General Medical Sciences, National Institutes of Health, and by New York State's Empire State Development Corporation (NYSTAR).

# **Author contributions**

R.T. and J.M.B. designed the study and analysed data. R.T. carried out directed evolution, molecular cloning, in cellular and in vitro activity assays, protein production and purification. S.R.B. and R.T. performed protein crystallization and X-ray data collection. S.R.B. analysed structural data. J.C.F. supervised X-ray crystallography analysis. R.T. and J.M.B. wrote the manuscript, with input from all authors.

# **Competing interests**

R.T. and J.M.B. are co-inventors on a patent application (PCT/ US2022/080999) filed by Cornell University for inventions related to super-active phospholipase Ds. The remaining authors declare no competing interests.

#### **Additional information**

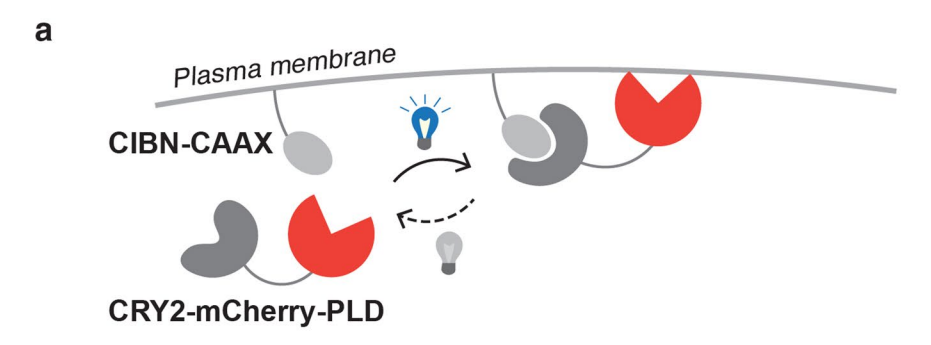
**Extended data** is available for this paper at https://doi.org/10.1038/s41557-023-01214-0.

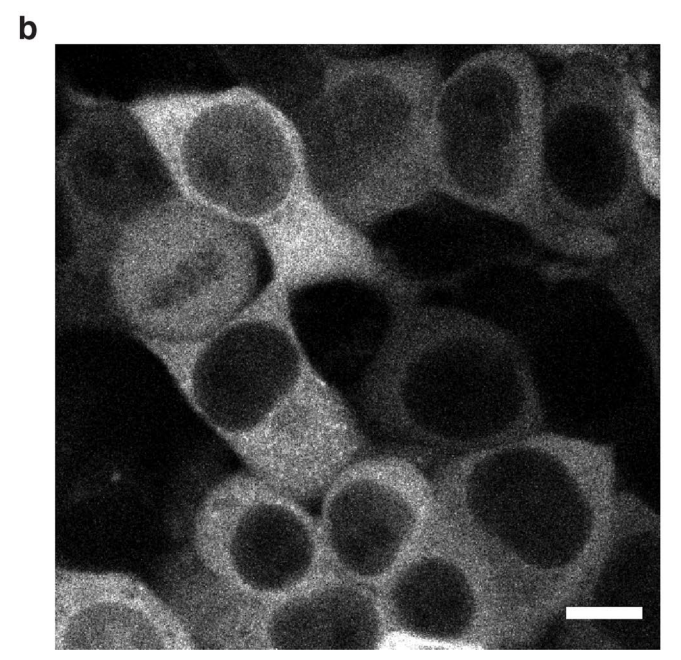
**Supplementary information** The online version contains supplementary material available at https://doi.org/10.1038/s41557-023-01214-0.

**Correspondence and requests for materials** should be addressed to Jeremy M. Baskin.

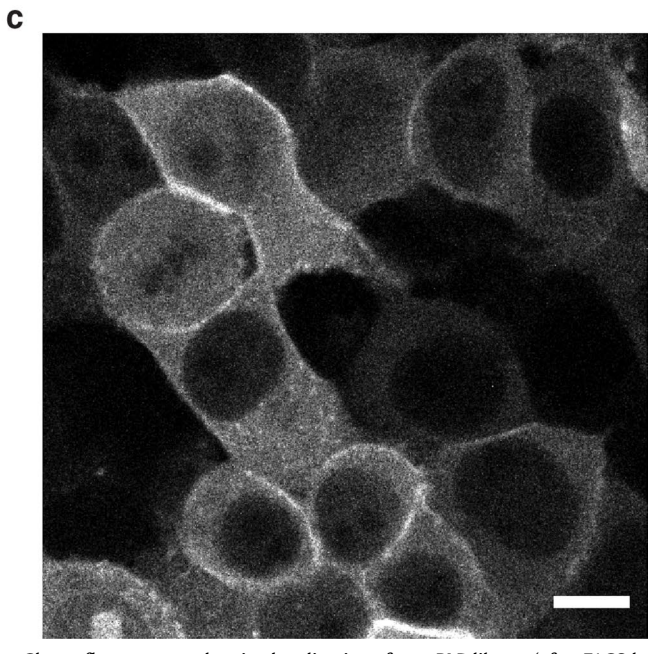
**Peer review information** *Nature Chemistry* thanks Bryan Dickinson and the other, anonymous, reviewer(s) for their contribution to the peer review of this work.

 $\label{lem:compression} \textbf{Reprints and permissions information} \ is \ available \ at \\ www.nature.com/reprints.$ 

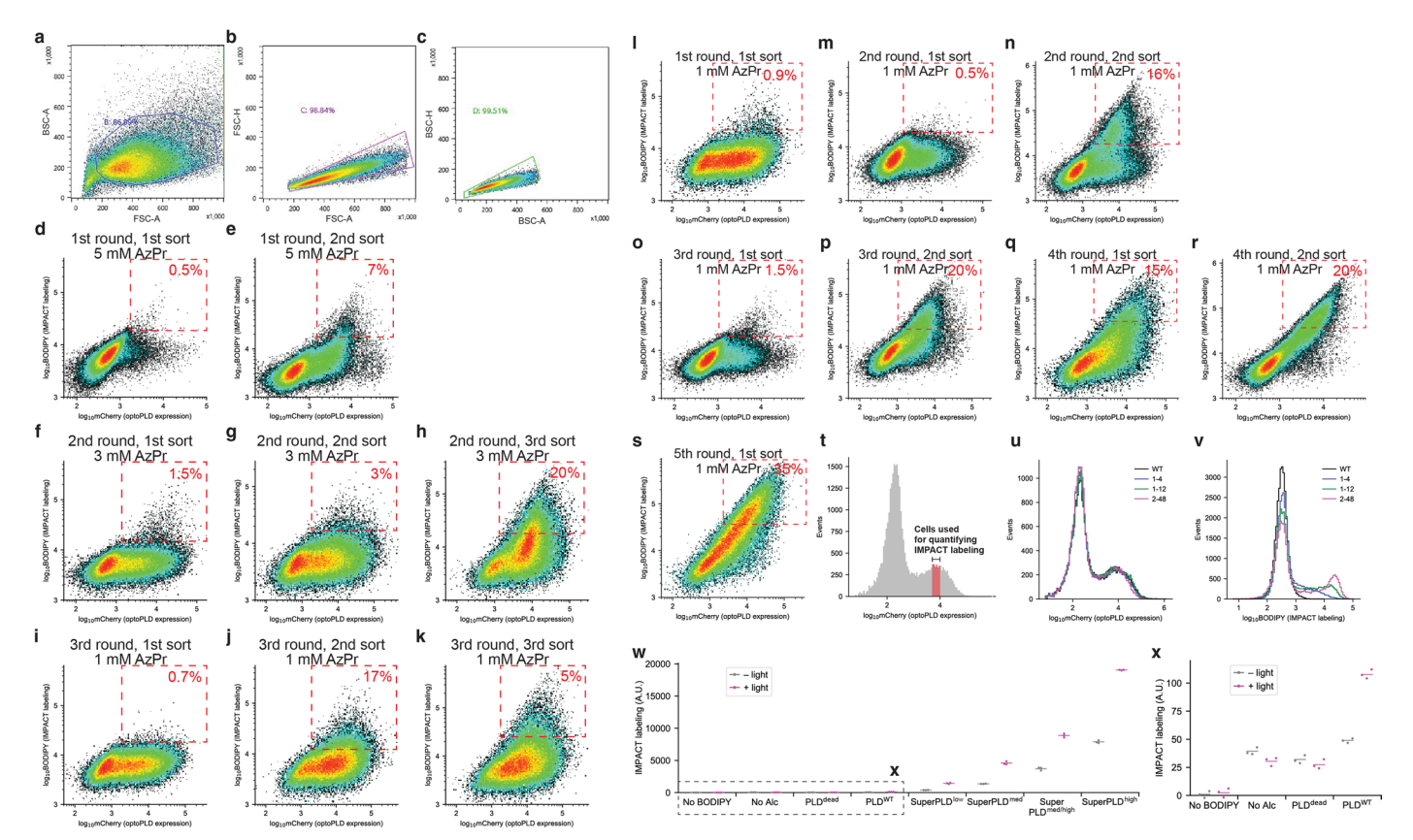




Extended Data Fig. 1 | A plasma membrane-targeted optoPLD library. a, Schematic depicting the design of plasma membrane-targeted optoPLD, which consists of CRY2-mCherry-PLD and CIBN-CAAX. OptoPLD-targeting membrane can be controlled by swapping the plasma membrane-targeted domain, CAAX, with another membrane-targeting domain.  $\mathbf{b} - \mathbf{c}$ , Confocal microscopy images of

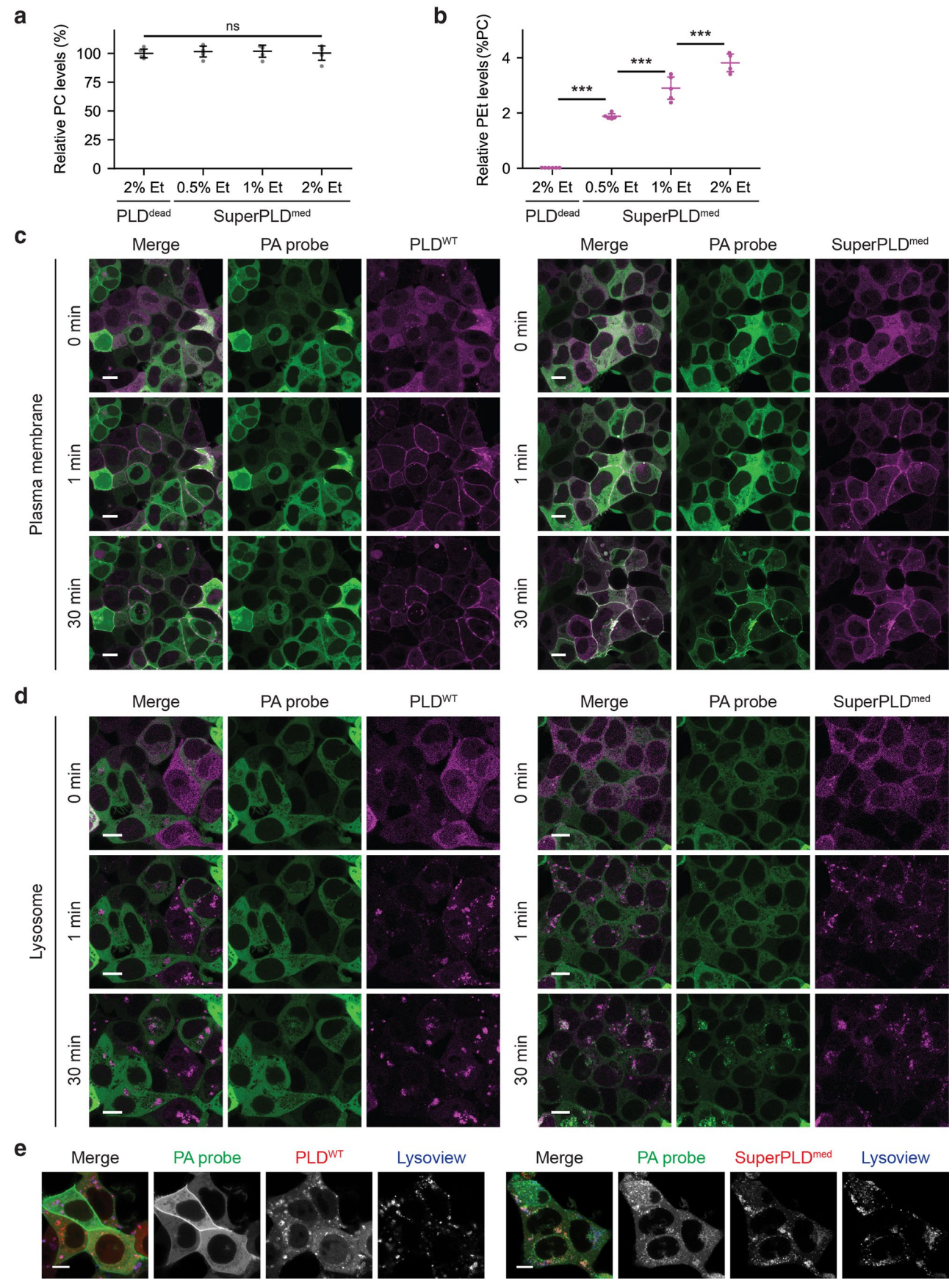


mCherry fluorescence showing localization of optoPLD library (after FACS-based selection) in HEK 293T cells before ( $\mathbf{b}$ ) and after ( $\mathbf{c}$ ) illumination with 488 nm light. The experiment was repeated for at least three times with similar results, and the representative images are shown. Scale bar: 10  $\mu$ m.



Extended Data Fig. 2 | FACS plot and gating strategy for each sorting of directed evolution and superPLD characterization by IMPACT. a-c, Gating strategy for sorting and analysis of HEK 293T cells expressing optoPLD mutants labelled by IMPACT. Plots of FSC-A vs. BSC-A, population B selected (a), FSC-A vs. FSC-H, population C selected (b), and BSC-A vs. BSC-H, population D selected (c) were used to gate for live, singlet cells. d-k, FACS plot of PLD library from each sorting in three rounds of selection with mutagenesis. l-s, FACS plot of PLD library from each sorting in five rounds of selection without mutagenesis. The round number, sort number within that round, concentration of azidopropanol (AzPr) used for IMPACT labelling, and the percentage of cells collected are indicated in each plot. t, Gating strategy for quantitative comparison of IMPACT labelling. The average BODIPY signal of cells with similar amount of mCherry signal (population shown in red, which is gated for an mCherry fluorescence

range of  $5\times10^3-1\times10^4$ ), was used. u-v, mCherry (u) and IMPACT labelling (v) histograms of cells expressing PLD<sup>WT</sup> (black), 1-4 (blue), 1-12 (green) and 2-48 (magenta), demonstrating that optoPLD mutants with different activity have similar expression levels. w-x, The effect of light stimuli on optoPLD activity. Cells expressing optoPLD were treated with 0.5 mM azidopropanol with or without intermittent blue light illumination, followed by treatment with 1  $\mu$ M BCN-BODIPY, and IMPACT fluorescence intensity normalized to optoPLD expression was determined by flow cytometry. Horizontal lines indicate average (n=3 independent transfection replicates) of mean intensities of IMPACT fluorescence. PLD<sup>dead</sup>, a catalytically dead PLD bearing the H167A mutation; PLD<sup>WT</sup>, wild-type PLD; superPLD<sup>low</sup>, superPLD mutant clone 1-4; superPLD<sup>med</sup>, superPLD mutant clone 1-12; superPLD mutant clone 1-27; superPLD mutant clone 2-48.

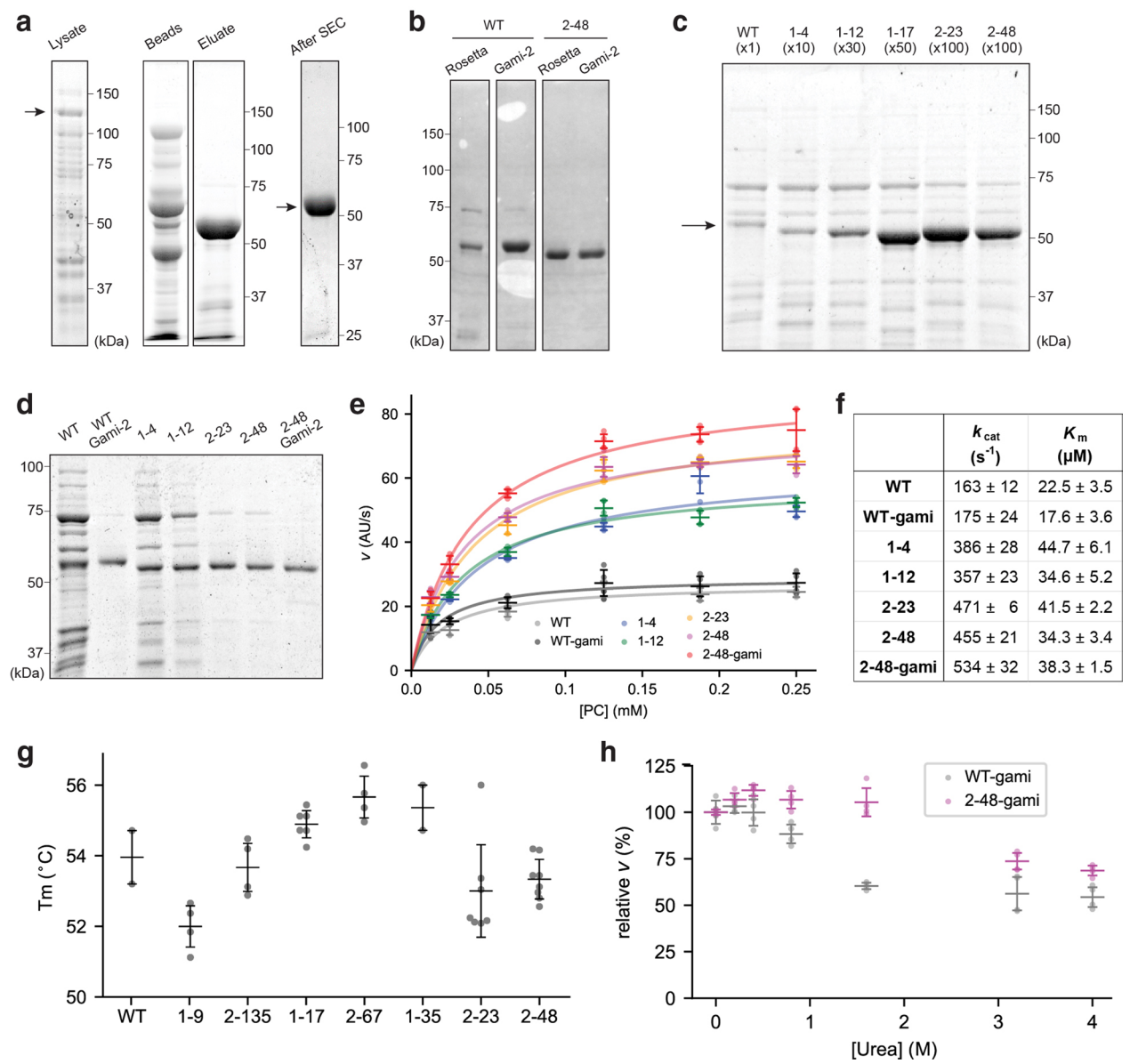


 $\label{lem:extended} \textbf{Extended Data Fig. 3} \, | \, \textbf{See next page for caption.}$ 

#### Extended Data Fig. 3 | Characterization of superPLD activity in cells.

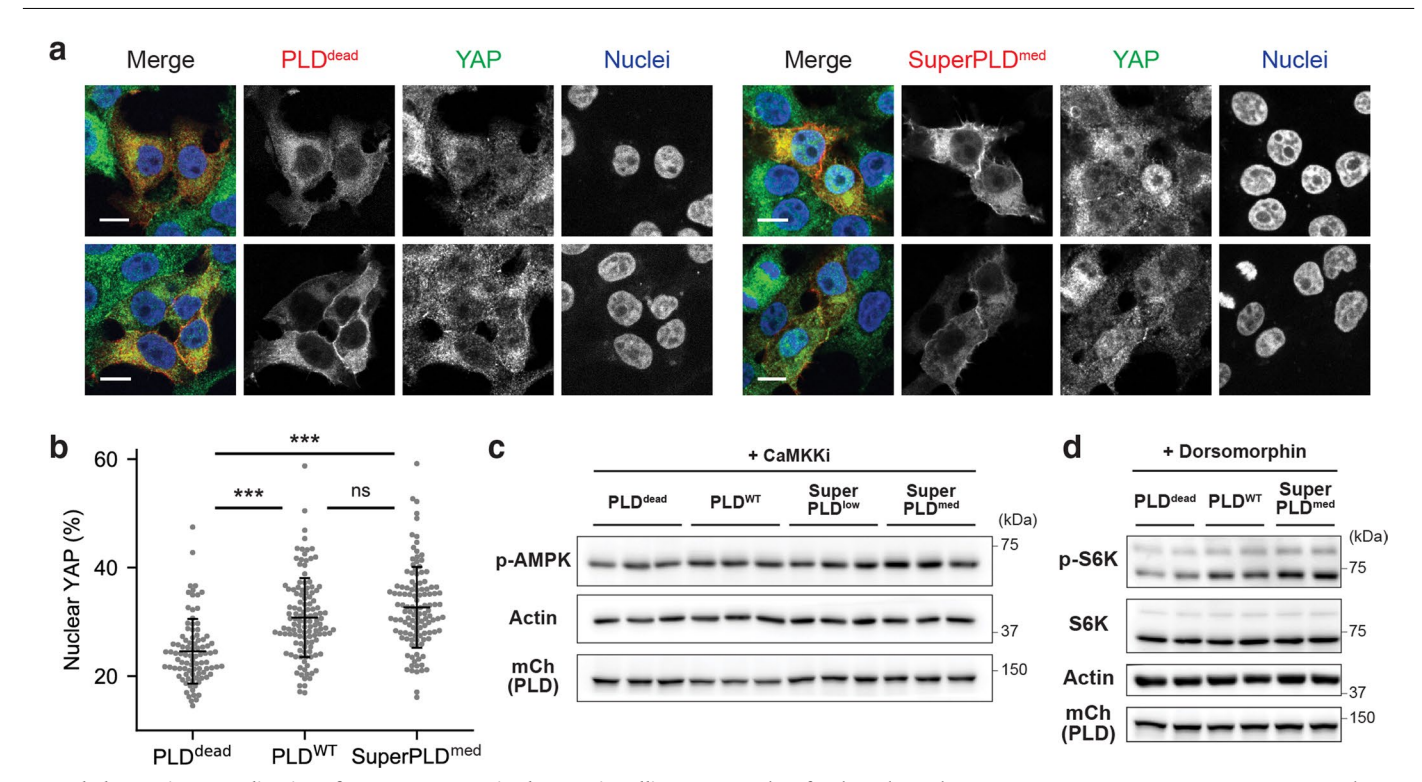
 $\label{eq:a-b} \textbf{Q} \textbf{u} \textbf{antification of substrate conversion by superPLD in cells. HEK 293T cells expressing plasma membrane-targeted optoPLD (superPLD^{med}) were treated with 0.5–2% ethanol (Et) for 30 min with intermittent blue light illumination. As a control, cells expressing PLD^{dead} were treated with 2% ethanol accordingly. The relative levels of the most abundant PLD substrate (16:0/18:1 PC; POPC) and its transphosphatidylation product (16:0/18:1 PEt; POPEt) were quantified by LC–MS. Relative PC levels compared to PC levels in control samples (PLD^{dead} expressing cells) (\textbf{a}) and relative PEt levels compared to PC levels (\textbf{b}) are plotted. Horizontal lines indicate average, and vertical error bars indicate standard deviation (n = 4 for superPLD^{med} with 2% ethanol and n = 5 for the others,$ 

and n refers to the number of biologically independent samples). Statistical significance was determined by one-way ANOVA followed by Sidak's multiple comparisons test. \*\*\*, p < 0.001. The p values for all the indicated pairwise comparisons in  $\mathbf{b}$  are < 0.0001.  $\mathbf{c}$ - $\mathbf{d}$ , Confocal microscopy images of HEK 293T cells co-expressing a PA probe (GFP-PASS) and optoPLD targeted to the plasma membrane ( $\mathbf{c}$ ) or lysosomes ( $\mathbf{d}$ ) before (0 min), immediately after (1 min), and 30 min after incubation with 488 nm light.  $\mathbf{e}$ , Confocal microscopy images of cells co-expressing the PA probe and the indicated optoPLD construct (WT or superPLD<sup>med</sup>) targeted to lysosomes, stained with LysoView 633. The experiment was repeated at least three times with similar results, and representative images are shown. Scale bars:  $10 \ \mu m$ .



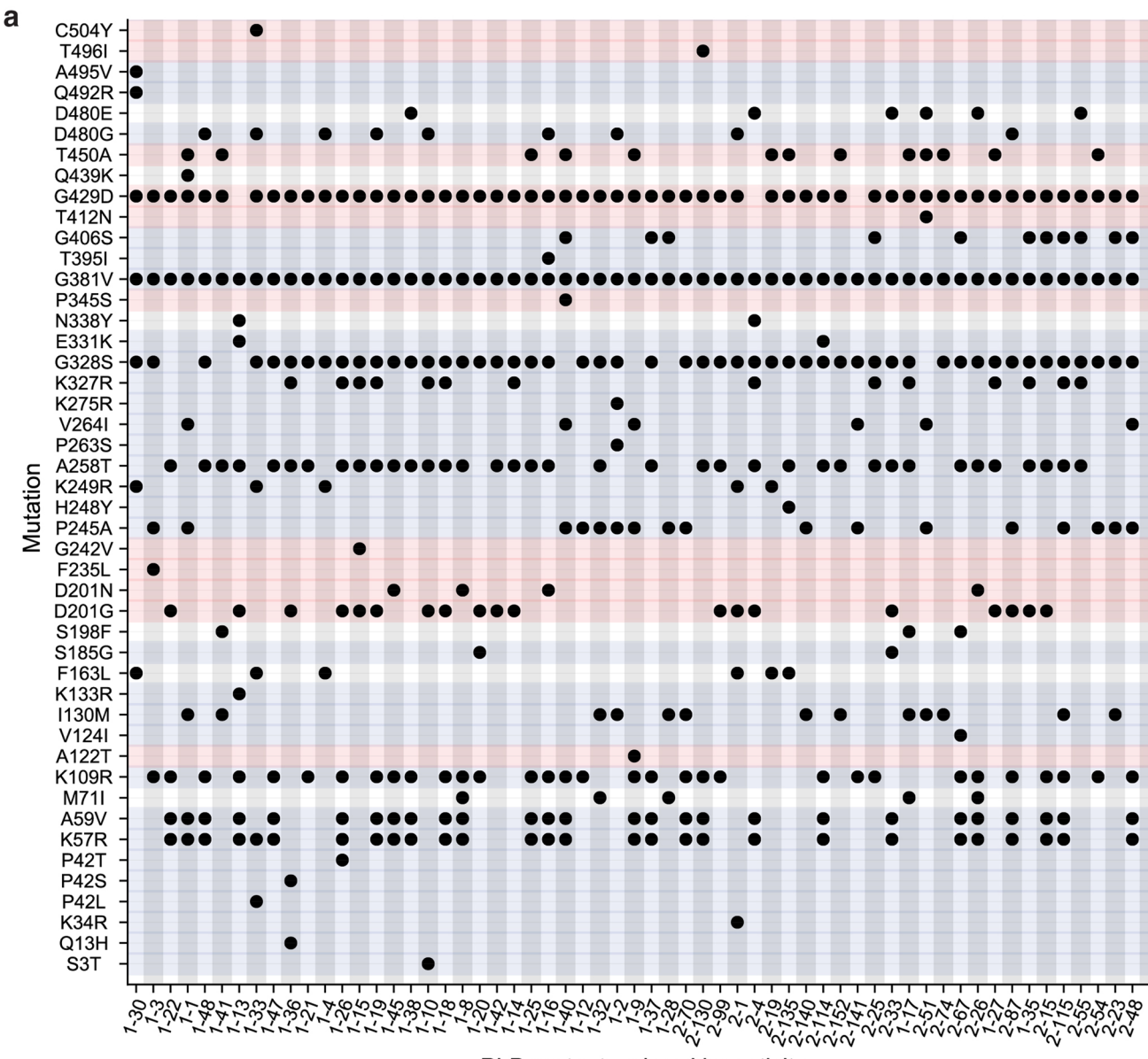
Extended Data Fig. 4 | Purification and in vitro characterization of superPLD and PLDWT. a, SDS-PAGE showing His-NusA-superPLD (shown here is clone 2-48) (113 kDa) in cell lysate, His-NusA (58 kDa) being retained on the TALON beads, and superPLD (55 kDa) eluting from the beads and exhibiting high purify after size-exclusion chromatography (SEC). 6xHis-NusA-superPLD was expressed in E.coli Rosetta 2 and purified using TALON resin. HRV 3C protease was used to cleave between NusA and PLD. Black arrows indicate the bands derived from PLD.  $\mathbf{b}$ , Ponceau stain with PLD<sup>WT</sup> and superPLD<sup>high</sup> purified from *Rosetta 2* vs. Gami-2 (Rosetta-gami 2) strains. When expressed in the Rosetta strain, PLDW1 showed substantial degradation and lower yield. c, SDS-PAGE showing general correlation between the activity of superPLD mutants in mammalian cells and the robustness of purification from E. coli. The numbers in parentheses indicate relative PLD activity in mammalian cells as determined by IMPACT (Fig. 2d). Black arrow indicates the bands corresponding to PLD. d-f, Kinetic analysis of PLD activity. PLDWT and a subset of superPLD mutants were diluted accordingly to adjust to equal amounts based on SDS-PAGE (d) and incubated with indicated concentration of DOPC. The purification of each PLD mutant was performed in at least three independent experiments (except for 1-4 and 1-12, which were purified in two independent experiments) with similar results, and the representative

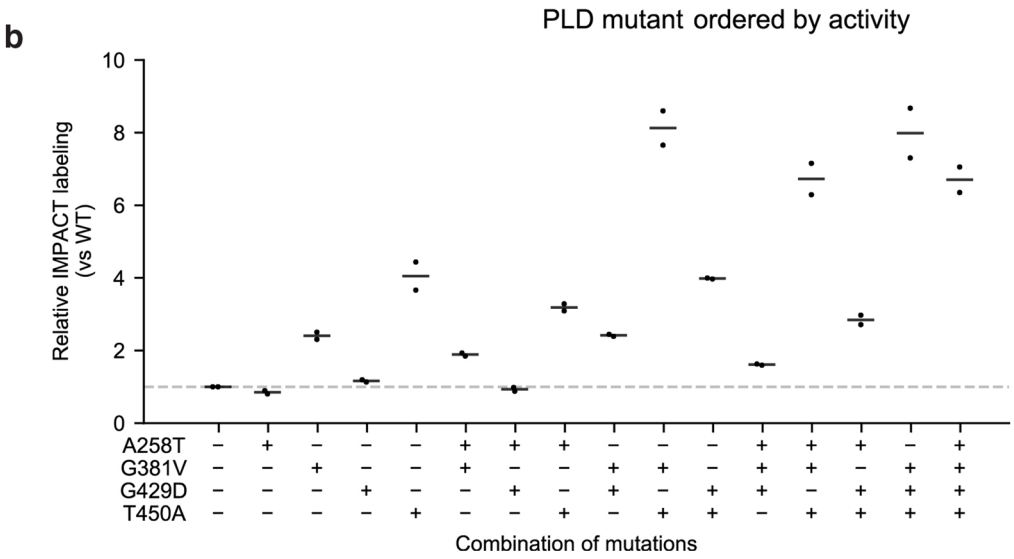
data are shown in panels a-d. Activity assays were performed using the Amplex Red Phospholipase D Assay Kit. The rates of reaction are plotted against the substrate concentration (e), and the data were fit to the Michaelis-Menten equation to obtain the kinetic parameters (f). Horizontal lines indicate average, and vertical error bars indicate standard deviation (n = 4 independent replicates). g, Thermal stability of PLDWT and a subset of superPLD mutants spanning a wide range of activities (see Fig. 2d), indicating no clear correlation between thermal stability and PLD activity. Melting temperature (Tm) was determined in a real-time thermocycler using SYPRO Orange dye. Horizontal lines represent the mean and error bars represent the standard deviation (n = 2, 4, 6, 2, 7, 8, and 4, respectively, and n refers to the number of independent replicates). h, Chemical stability of PLDWT and superPLDhigh (2-48) purified from the Gami-2 strain, indicating increased chemical stability for superPLD. Each enzyme was incubated with indicated concentration of urea in PBS for 12 h at 37 °C. followed by an activity assay using the Amplex Red Phospholipase D Assay Kit. Relative rates of reaction compared to control samples (enzymes incubated in PBS only) are plotted. Horizontal lines indicate average, and vertical error bars indicate standard deviation (n = 4 independent replicates).



**Extended Data Fig. 5** | **Application of superPLD to manipulate PA signalling. a**-**b**, Quantification of nuclear YAP levels to evaluate Hippo signalling activity. HEK 293T cells expressing plasma membrane-targeted optoPLD (PLD dead, PLD WT or superPLD med) were immunostained for YAP (**a**; scale bars:  $10 \mu m$ ), and percentage of the total YAP signal that is colocalized with the DAPI (nucleus) signal is plotted for each transfected cell (**b**). Horizontal lines indicate average, and vertical error bars indicate standard deviation (n = 92,122, and 119, respectively, and n refers to the number of cells examined over three independent experiments). Statistical significance was determined by one-way ANOVA followed by Sidak's multiple comparisons test. \*\*\*, p < 0.001. The

p values for the indicated pairwise comparisons are <0.0001, <0.0001, and 0.14, respectively.  $\mathbf{c}$ , Representative Western blots used to quantify p-AMPK levels (see Fig. 5d). Cells expressing plasma membrane-targeted optoPLD were treated with a CaMKK inhibitor (STO-609) for 6 h to block CaMKK-mediated AMPK activation, followed by a 30 min incubation with 488 nm light.  $\mathbf{d}$ , Representative Western blots used to quantify p-S6K levels (see Fig. 5e). Cells expressing plasma membrane-targeted optoPLD were treated with an AMPK inhibitor (dorsomorphin) for 1 h, followed by a 30 min incubation with 488 nm light. Experiments were repeated at least three times with similar results for  $\mathbf{c}$  and  $\mathbf{d}$ .



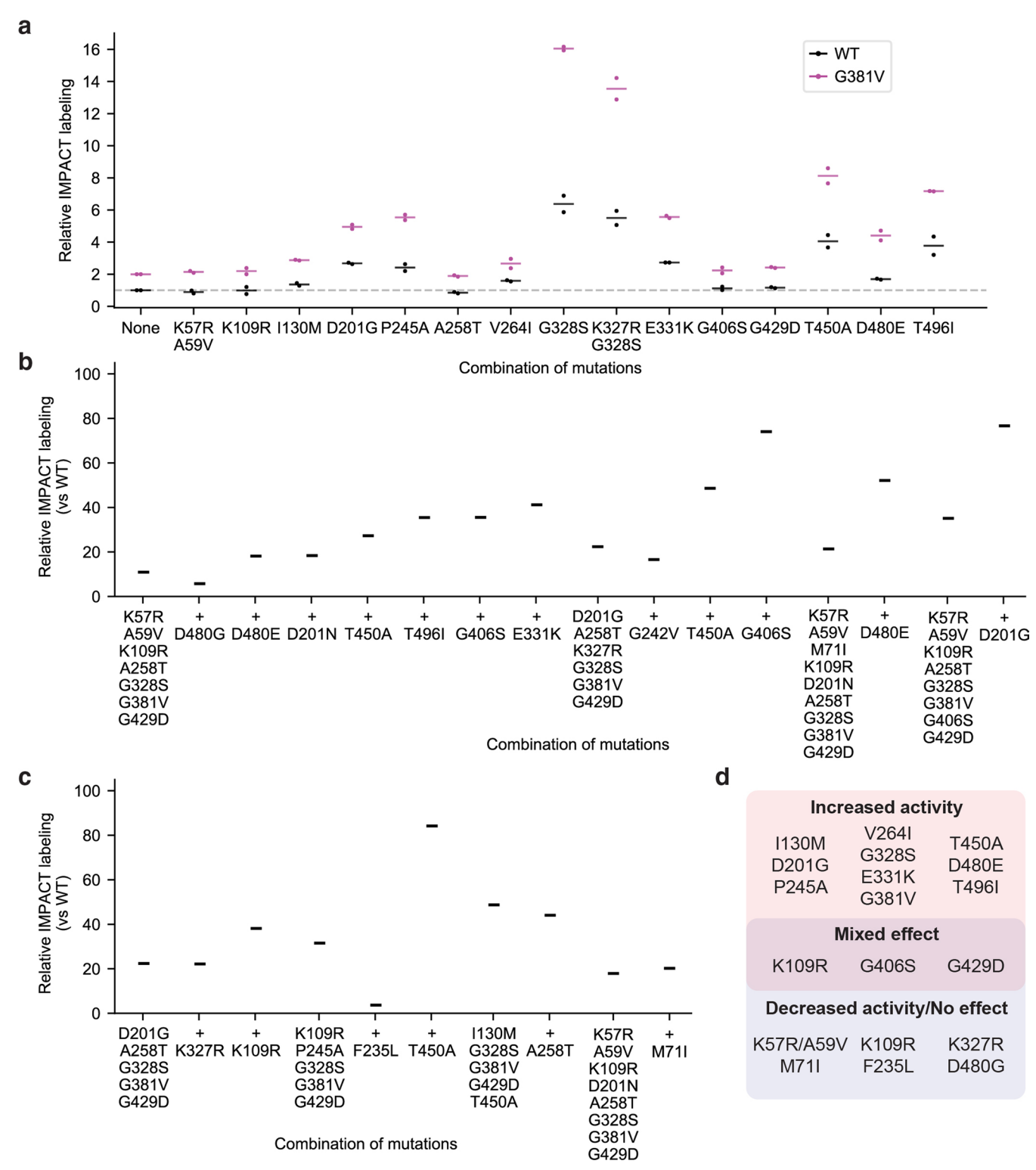


Extended Data Fig. 6 | See next page for caption.

#### Extended Data Fig. 6 | Mutations identified in various superPLD clones.

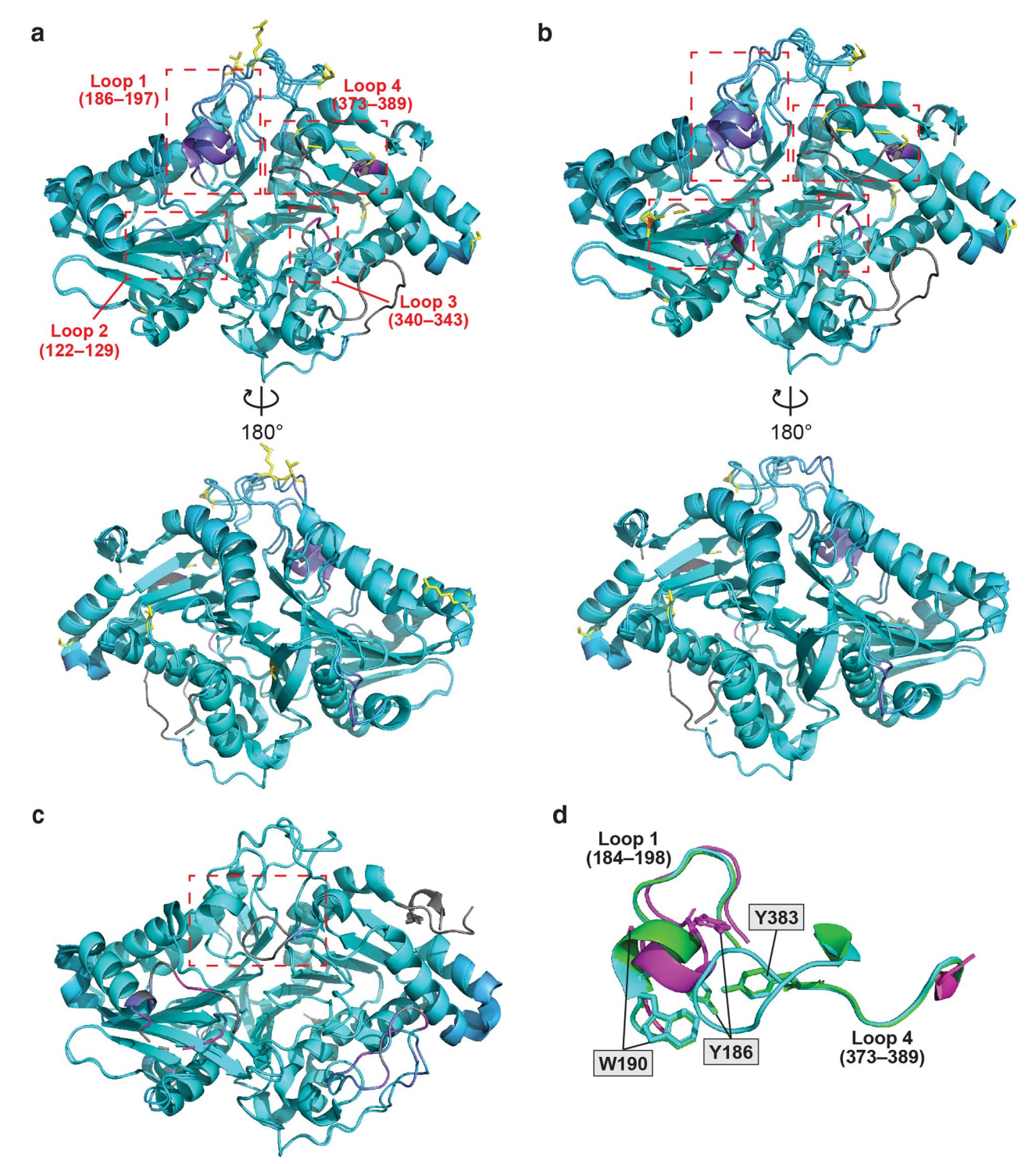
**a**, PLD mutant clones are shown in order of PLD activity in cells determined by IMPACT (increasing from left to right), and black dots indicate the presence of a particular point mutation in that PLD mutant. Mutants with identical sets of mutations are not shown in the plot. The mutated residues are coloured based on conservation across PLDs from different species, determined by ConSurf;<sup>1-3</sup> red: high conservation, white: medium, blue: low. **b**, Activity assay of PLD mutants containing different combinations of four commonly occurring mutations that were generated in the PLD<sup>WT</sup> background (A258T, G381V, G429D and T450A). Cells expressing plasma membrane-targeted optoPLD with the indicated set of

mutations were labelled with IMPACT using 1 mM azidopropanol and 1  $\mu$ M BCN-BODIPY. IMPACT fluorescence intensity normalized to optoPLD expression was determined by flow cytometry, and the relative values for each mutant compared to the PLD  $^{WT}$  are plotted as relative IMPACT labelling (n = 2 independent transfection replicates). The effect of each mutation occurred mostly in a combinatorial manner (that is, most mutations exhibited multiplicative effects in either increasing (G381V, T450A) or slightly decreasing (A258T) the activity, though G429D slightly increased activity alone but had negligible effects when combined with other mutations).

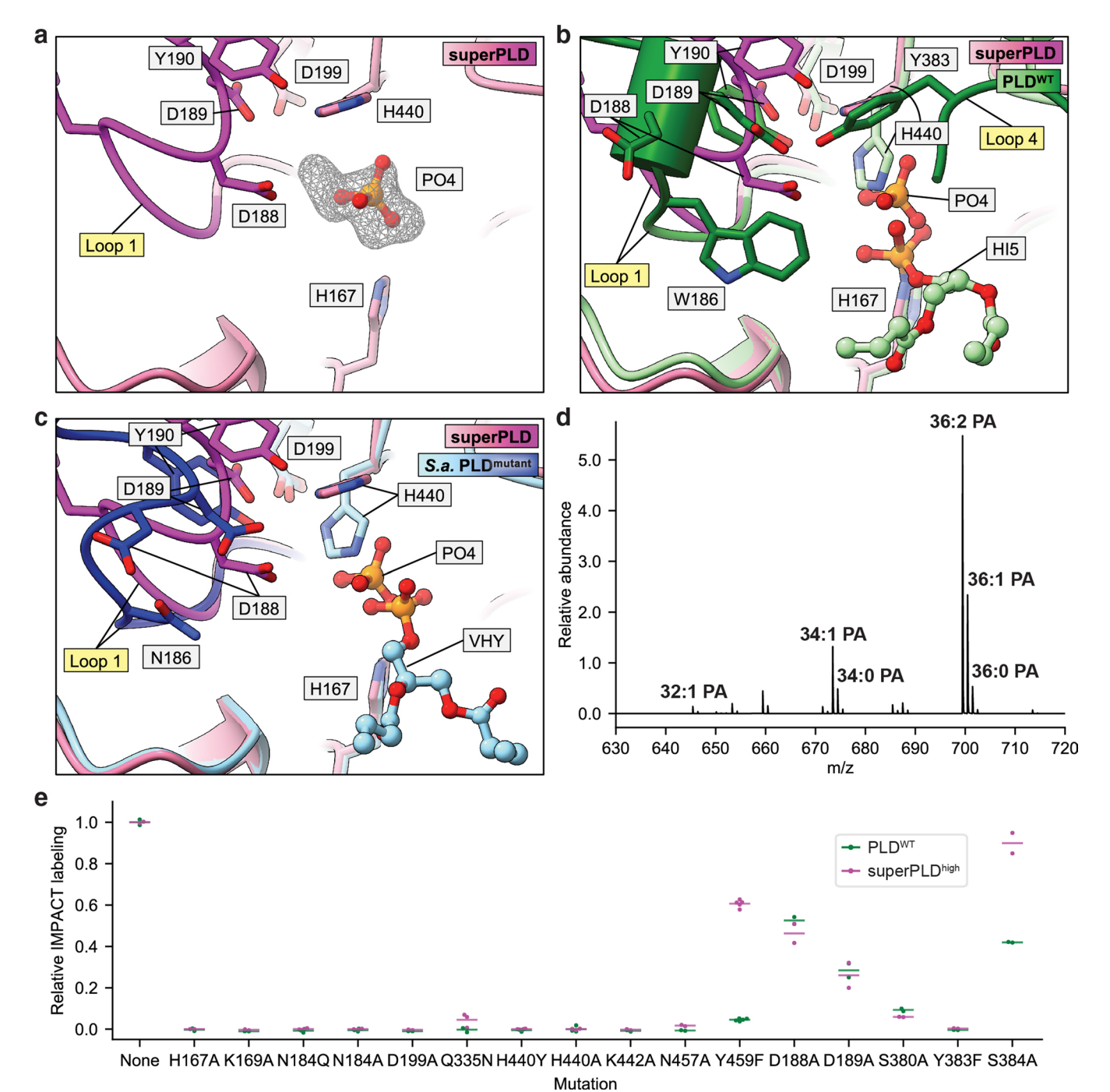


**Extended Data Fig. 7** | **Analysis of the effects of acquired mutations on PLD activity. a**, Relative activity of PLDs with frequently occurring mutations that were individually installed into either the PLDWT (black) or G381V (magenta) background. Cells were labelled and analysed by flow cytometry as described in Extended Data Fig. 6. Horizontal lines indicate average (n = 2 independent transfection replicates) of relative mean intensities of IMPACT fluorescence. Dashed grey lines indicate the activity of PLDWT, which is normalized to 1. **b-c**, Systematic comparison to evaluate the effect of individual mutations in

the context of actual superPLD mutants isolated from the screen. The graphs show related mutants grouped separately. Each group contains a "template mutant" consisting of a specific set of mutations (which came from directed evolution experiments), which is shown left-most within each group, as well as other mutants that contain all the mutations in the template mutant plus one additional mutation that is indicated. **d**, Three different types of effects caused by individual mutations, determined based on point mutation analysis and systematic comparison analysis of mutants.



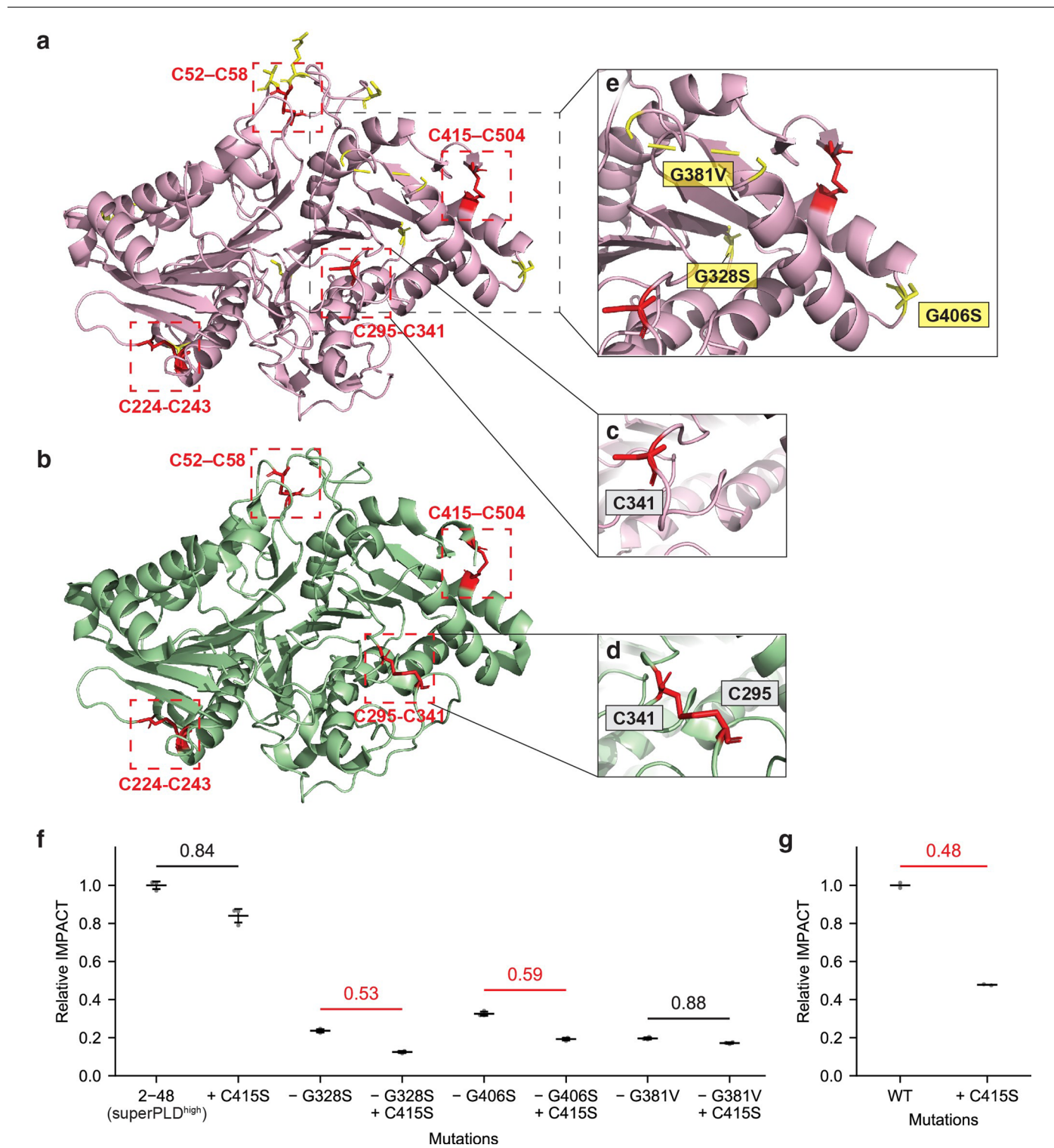
Extended Data Fig. 8 | Mapping correlations between structural shifts and mutated sites in superPLDs. a–b, Alignments of PLDWT with either superPLDhigh (2-48) (a) or superPLD clone 2-23 (b), with the differences between the two structures coloured by root mean square deviation (RMSD) using the ColorByRMSD script  $^4$ . The distances between aligned C $\alpha$  atom pairs are stored as B-factors of these residues, which are coloured by a colour spectrum, with cyan specifying the minimum pairwise RMSD and magenta indicating the maximum. Unaligned residues are coloured grey. Sites of mutations in each superPLD are shown in yellow, and mutated residues are shown as yellow sticks except for G381V, which exists on the missing flexible loop that is shown as a yellow dashed



#### $\textbf{Extended Data Fig. 9} \, | \, \textbf{Analysis of the active site structure of superPLD.} \\$

**a-c**, Structures of the active sites of superPLD<sup>high</sup> (2-48) (**a**), superPLD<sup>high</sup> overlaid with PLD WT (PDB ID: 1VOY; green) (**b**), and superPLD<sup>high</sup> overlaid with PLD from *Streptomyces antibioticus* engineered to produce phosphatidylinositol (PDB ID: 7JRV; light blue) (**c**). Loops 1 and 4 in each structure are shown in dark purple (superPLD 2-48) and dark blue (engineered *S. antibioticus* PLD). A phosphate ligand is modelled in the electron density found in the active site of superPLD<sup>high</sup>. Polder omit map for the region around the modelled phosphate molecule is shown as a mesh, contoured at 0.52  $\sigma$  using a carve distance of 3 Å d. **d**, LC-MS analysis of a lipid extract from purified superPLD, demonstrating the existence of multiple PA species that co-purified with superPLD<sup>high</sup> (2-48). **e**, Comparison of the effects of site-directed mutation on PLD<sup>WT</sup> (green) vs. superPLD<sup>high</sup> (2-48;

magenta). HEK 293T cells expressing plasma membrane-targeted optoPLD versions of PLD^{WT} or superPLD^{high} (2-48) with the indicated point mutation were labelled with 10 mM (for PLD^{WT}) or 100  $\mu$ M (for superPLD^{high}) azidopropanol, followed by click chemistry tagging with 1  $\mu$ M BCN-BODIPY. IMPACT fluorescence intensity normalized to optoPLD expression was determined by flow cytometry, and the relative values for each mutant compared to the appropriate parental PLD (that is, PLD^{WT} or superPLD^{high} (2-48)) are plotted as relative IMPACT labelling. Plots are replicates (n = 5 for Y459F, n = 3 for N184Q, N184A, Q335N, H440Y and H440A, n = 2 for the others, and n refers to the number of independent transfection replicates) from flow cytometry analysis, and the line indicates the average.



**Extended Data Fig. 10** | **Disulfide bonds in superPLD and PLD**<sup>WT</sup> **structures. a**–**e**, Crystal structures of superPLD<sup>high</sup> (2-48) (**a**, **c**, **e**) and PLD<sup>WT</sup> (PDB ID: 1VOY) (**b**, **d**) with cysteine residues shown in red. Disulfide bonds in PLD<sup>WT</sup> are highlighted with red dashed boxes. In superPLD structures, C295 was not resolved, and C341 residue was flipped, indicating that the C295–C341 disulfide bond is reduced. Sites of mutations in superPLD<sup>high</sup> are shown in yellow, with mutated residues shown as yellow sticks (except for G381V, which is in an unresolved flexible loop and is shown as a yellow dashed line). **f**–**g**, Identification of a mutation in superPLD that is responsible for enhanced tolerance to disabled disulfide bond formation. Mutations in superPLD<sup>high</sup> (2-48) that occur at three

positions near C415 (G328S, G381V, and G406S) were, within the superPLD  $^{\rm high}$  (2-48) background, reverted to the residue that occurs in PLD  $^{\rm WT}$ , and the relative effects of the C415S mutation on PLD activity in these constructs (**f**) were compared to the effect of the C415S mutation in PLD  $^{\rm WT}$  (**g**). IMPACT fluorescence intensity normalized to optoPLD expression was determined by flow cytometry. Horizontal lines indicate average (n = 3 independent transfection replicates) of relative mean intensities of IMPACT fluorescence of cells expressing the indicated mutant PLD compared to the parental PLD (for example, PLD  $^{\rm WT}$  or superPLD  $^{\rm high}$  (2-48)), as measured by flow cytometry.

# nature research

Corresponding author(s):	Jeremy M. Baskin		
Last updated by author(s):	2023/2/22		

# **Reporting Summary**

Nature Research wishes to improve the reproducibility of the work that we publish. This form provides structure for consistency and transparency in reporting. For further information on Nature Research policies, see our Editorial Policies and the Editorial Policy Checklist.

For all statistical analyses, confirm that the following items are present in the figure legend, table legend, main text, or Methods section.

o.			
۲	at	121	ICS

n/a	Confirmed			
	The exact sample size (n) for each experimental group/condition, given as a discrete number and unit of measurement			
	A statement on whether measurements were taken from distinct samples or whether the same sample was measured repeatedly			
	The statistical test(s) used AND whether they are one- or two-sided  Only common tests should be described solely by name; describe more complex techniques in the Methods section.			
$\boxtimes$	A description of all covariates tested			
	A description of any assumptions or corrections, such as tests of normality and adjustment for multiple comparisons			
	A full description of the statistical parameters including central tendency (e.g. means) or other basic estimates (e.g. regression coefficient) AND variation (e.g. standard deviation) or associated estimates of uncertainty (e.g. confidence intervals)			
	For null hypothesis testing, the test statistic (e.g. <i>F</i> , <i>t</i> , <i>r</i> ) with confidence intervals, effect sizes, degrees of freedom and <i>P</i> value noted <i>Give P values as exact values whenever suitable.</i>			
$\boxtimes$	For Bayesian analysis, information on the choice of priors and Markov chain Monte Carlo settings			
$\boxtimes$	For hierarchical and complex designs, identification of the appropriate level for tests and full reporting of outcomes			
	Estimates of effect sizes (e.g. Cohen's $d$ , Pearson's $r$ ), indicating how they were calculated			
	Our web collection on <u>statistics for biologists</u> contains articles on many of the points above.			
So	ftware and	d code		
Poli	cy information a	about <u>availability of computer code</u>		
Da	ta collection	Zeiss Zen Blue 2.3, Sony MA900, BD FACSDiva, BioTek Gen5, Agilent MassHunter, Roche LightCycler 480, Bio-Rad ChemiDoc MP System, ÄKTA pure, Advanced Photon Source, Cornell High Energy Synchrotron Source		
Da	nta analysis	Python (custom codes provided as SI), ImageJ, COOT, PHENIX, Microsoft Excel		

# Data

Policy information about availability of data

All manuscripts must include a data availability statement. This statement should provide the following information, where applicable:

For manuscripts utilizing custom algorithms or software that are central to the research but not yet described in published literature, software must be made available to editors and reviewers. We strongly encourage code deposition in a community repository (e.g. GitHub). See the Nature Research guidelines for submitting code & software for further information.

- Accession codes, unique identifiers, or web links for publicly available datasets
- A list of figures that have associated raw data
- A description of any restrictions on data availability

Structural models and structure factors of superPLD (2-48) and superPLD (2-23) have been deposited in the RCSB PDB with the accession numbers 8CTQ and 8CTP, respectively. The structural model of PLDWT is available in RCSB PDB with the accession number 1V0Y. SuperPLD plasmids used for this study have been deposited in Addgene (https://www.addgene.org/browse/article/28229113/). Other data supporting the findings of this study are available within the Article and the Supplementary Information. Source data are provided with this paper.

Field-spe	ecific reporting			
Please select the or	ne below that is the best fit for your research. If you are not sure, read the appropriate sections before making your selection.			
∑ Life sciences	Behavioural & social sciences Ecological, evolutionary & environmental sciences			
For a reference copy of t	the document with all sections, see <u>nature.com/documents/nr-reporting-summary-flat.pdf</u>			
Life scier	nces study design			
All studies must dis	close on these points even when the disclosure is negative.			
Sample size	All the experiments were performed with at least three biological replicates except for quantitative comparison of PLD mutants' activity by flow cytometry, in which case the readout is average fluorescent signal of a cell population (n>100) expressing PLD mutants.			
Data exclusions	lusions None			
Replication	Findings were replicated as indicated in each figure legend.			
Randomization	Allocation of samples into groups was random.			
Blinding	All data were analyzed systematically by either Python, ImageJ, COOT, PHENIX, or Microsoft Excel. For this reason, it was determined that sample blinding was not necessary for the experiments in this study.			
Reportin	g for specific materials, systems and methods			
·	on from authors about some types of materials, experimental systems and methods used in many studies. Here, indicate whether each material, ted is relevant to your study. If you are not sure if a list item applies to your research, read the appropriate section before selecting a response.			
Materials & exp	perimental systems Methods			
n/a Involved in th	n/a Involved in the study			
Antibodies	ChIP-seq			
Eukaryotic	cell lines			
Palaeontol	ogy and archaeology MRI-based neuroimaging			
Animals an	d other organisms			
Human research participants				
Clinical data				
Dual use research of concern				
A				
Antibodies				
Antibodies used	Phospho-AMPKα (Thr172) (Cell Signaling Technology; #2535), phospho-p70 S6 kinase (Thr389) (Cell Signaling Technology; #9205), p70 S6 kinase (Santa Cruz Biotechnology; sc-8418), mCherry (Novus Biologicals; NBP1-96752), and actin (MP Biomedicals; 08691001)			
Validation	All the antibodies were validated by validation statements on the manufacturer's website and relevant citations.			
Eukaryotic c	ell lines			
Policy information				
. 3.10, 1.110111111111111111				

Cell line source(s)

HEK 293T cells were obtained from ATCC; HEK 293TN cells were obtained from the Bretscher lab (Cornell).

Authentication

Cell lines were not authenticated

Mycoplasma contamination

Commonly misidentified lines (See ICLAC register)

None

# Flow Cytometry

# **Plots**

Confirm that:

- The axis labels state the marker and fluorochrome used (e.g. CD4-FITC).
- The axis scales are clearly visible. Include numbers along axes only for bottom left plot of group (a 'group' is an analysis of identical markers).
- All plots are contour plots with outliers or pseudocolor plots.
- A numerical value for number of cells or percentage (with statistics) is provided.

# Methodology

Sample preparation

HEK 293T cells were transfected with mCherry-tagged superPLDs and labeled via IMPACT with BODIPY fluorophores, rinsed, and analyzed live.

Sony MA900 Cell Sorter and FACSAria Fusion Cell Sorter

Software

Sony MA900 and BD FACSDiva

SOTEWATE SOTI WASOO and BUT ACSDIVA

Cell population abundance Post-sort fractions were re-seeded onto new cell culture plates and grown back to normal population, confirming the lack of contamination and allowing only viable, growing cells to be carried onto subsequent analysis.

Gating strategy

FSC-A vs. BSC-A was used to gate for live cells, and FSC-A vs. FSC-H and BSC-A vs. BSC-H were used to gate for singlet cells.

mCherry and BODIPY signals were used to gate for cells expressing optoPLD with high activity.

| Tick this box to confirm that a figure exemplifying the gating strategy is provided in the Supplementary Information.